CHARLES UNIVERSITY
FACULTY OF PHARMACY IN HRADEC KRÁLOVÉ
DEPARTMENT OF PHARMACOLOGY AND TOXICOLOGY

RHEINISCHE FRIEDRICH-WILHELMS-UNIVERSITÄT BONN
FACULTY OF MATHEMATICS AND NATURAL SCIENCES
DEPARTMENT OF PHARMACEUTICAL CHEMISTRY

KINETIC EVALUATION OF POTENTIAL INHIBITORS FOR SELECTED CYSTEINE PROTEASES

HODNOCENÍ VLIVU POTENCIÁLNÍCH INHIBITORŮ VYBRANÝCH CYSTEINOVÝCH PROTEÁZ NA JEJICH KINETICKÉ VLASTNOSTI

MASTER'S THESIS

SUPERVISOR: RNDR. JAKUB HOFMAN, PH.D.
CONSULTANTS: CARINA LEMKE
PROF. DR. MICHAEL GÜTSCHOW

HRADEC KRÁLOVÉ 2020

ANNA ODVÁRKOVÁ

DECLARATION

I hereby declare that this thesis is my own original work. All the literature and other sources used for writing this thesis are listed in the reference section and are thoroughly cited throughout the work. In addition, I affirm that this work has not been used to obtain the same or another degree.

Hradec Králové ……..

ACKNOWLEDGEMENTS

I express my sincere appreciation to Prof. Dr. Michael Gütschow for giving me the opportunity to join his group and carry out the research at the Rheinische Friedrich-Wilhelms-Universität Bonn. He introduced me into the topic and supported me throughout the process.

I would like to thank RNDr. Jakub Hofman, Ph.D. for his help, advice and the supervision at my home university in the Czech Republic.

My special thanks belong to Carina Lemke for being the best motivational leader, providing me precise guidance, enthusiastic encouragement and useful critiques of this thesis.

I am very grateful to all my departmental colleagues for welcoming environment and making my time at the university more than pleasant.

I would also like to acknowledge Erasmus+ Programme of the European Union together with Erasmus Student Network Bonn for a wonderful experience in Germany.

Last but not least, I wish to thank my family and friends for their immense support throughout my studies.

ABSTRACT

Charles University
Faculty of Pharmacy in Hradec Králové
Department of Pharmacology and Toxicology
Student: Anna Odvárková
Supervisor: RNDr. Jakub Hofman, Ph.D.
Consultants: Carina Lemke
Prof. Dr. Michael Gütschow
Title of diploma thesis: Kinetic Evaluation of Potential Inhibitors for Selected Cysteine Proteases

Cysteine cathepsins are proteases which are naturally present in the human body, taking part in various physiological processes such as cell signaling, proliferation or bone remodeling. However, their dysregulation leads to serious disorders. An aberrant activity of cysteine cathepsins is present in diseases like cancer, osteoporosis, neurodegenerative disorders or autoimmune diseases. Therefore, these enzymes can serve as valuable diagnostic or therapeutic targets. Rhodesain is a parasitic protease produced by *Trypanosoma brucei rhodesiense* and essential for its survival. This enzyme shares a high homology with human cysteine cathepsin L. Inhibition of rhodesain can be a potential treatment of African trypanosomiasis, also known as sleeping sickness.

Inhibitory potency of several compounds against the target enzymes was assayed spectrophotometrically or fluorometrically and the results were evaluated by using linear or non-linear regression. Determination of a Michaelis-Menten constant for rhodesain under specific assay conditions was also performed. Some potent inhibitors of tested proteases have been identified and additionally, a potential activity-based probe was investigated for its applicability in sodium dodecyl sulfate polyacrylamide gel electrophoresis.

ABSTRAKT

Univerzita Karlova
Farmaceutická fakulta v Hradci Králové
Katedra farmakologie a toxikologie
Studentka: Anna Odvárková
Školitel: RNDr. Jakub Hofman, Ph.D.
Dohlížející: Carina Lemke
Prof. Dr. Michael Gütschow

Název diplomové práce: Hodnocení vlivu potenciálních inhibitorů vybraných cysteinových proteáz na jejich kinetické vlastnosti

Cysteinové katepsíny jsou proteázy, které se přirozeně vyskytují v lidském těle a účastní se mnoha fyziologických procesů, jako je například buněčná signalizace, proliferace nebo kostní přestavba. Jejich dysregulace ale může vést k vážným poruchám. Abnormální aktivita cysteinových katepsínů je přítomna u onemocnění zahrnujících osteoporózu, nádorová, neurodegenerativní nebo autoimunitní onemocnění. Tyto enzymy proto mohou sloužit jako hodnotné diagnostické nebo terapeutické cíle. Rodesain je parazitická proteáza produkovaná *Trypanosomou brucei rhodesiense* a je nezbytná pro její přežití. Tento enzym sdílí vysokou homologii s lidským cysteinovým katepsinem L. Inhibice rodesainu může být potenciální léčbou africké trypanosomiázy, také známé jako spavé nemoci.

Inhibiční potenciál mnoha sloučenin proti cílovým enzymům byl testován spektrofotometricky nebo fluorometricky a výsledky byly hodnoceny za použití lineární či nelineární regrese. Také bylo provedeno stanovení konstanty Michaelise a Mentenové pro rodesain za specifických testovacích podmínek. Bylo identifikováno pár silných inhibitorů testovaných proteáz a dodatečně byla testována použitelnost potenciální sondy značící aktivní enzym v elektroforéze v polyakrylamidovém gelu v přítomnosti dodecylsíranu sodného.

CONTENTS

1. ABBREVIATIONS

ABP	activity-based probe
AMC	7-amino-4-methylcoumarin
APS	ammonium persulfate
Arg	arginine
Brij 35	polyethylene lauryl ether
Cat B	cathepsin B
Cat K	cathepsin K
Cat L	cathepsin L
Cat S	cathepsin S
CHAPS	3-[(3-cholamidopropyl)dimethylammonio]-1-propanesulfonate
DMSO	dimethylsulfoxide
DTT	dithiothreitol
E	enzyme
E-64	L-trans-epoxysuccinyl-leucylamido(4-guanidino)butane
EDTA	ethylenediaminetetraacetic acid
HEK	human embryonic kidney
[I]	inhibitor concentration
I	inhibitor
IC_{50}	half maximal inhibitory concentration
K_i	inhibitory constant
k_{inact}	inactivation rate constant
k_{inact}/K_i	second-order inactivation rate constant
K_M	Michaelis-Menten constant
k_{obs}	first-order rate constant
k_{off}	dissociation constant
k_{on}	association constant
k_{on}'	apparent association constant
Leu	leucine
MES	2-(*N*-morpholino)ethanesulfonic acid
NI	no inhibition
[P]	product concentration

P	product
Phe	phenylalanine
pNA	*para*-nitroaniline
RA	remaining enzyme activity
Rhod	rhodesain
[S]	substrate concentration
S	substrate
SDS	sodium dodecyl sulfate
SDS-PAGE	sodium dodecyl sulfate polyacrylamide gel electrophoresis
T. b.	*Trypanosoma brucei*
TRIS	tris(hydroxymethyl)aminomethane
Triton	polyethylene glycol *p*-(1,1,3,3-tetramethylbutyl)-phenyl ether
UV	ultraviolet
v_0	reaction rate in the absence inhibitor
Val	valine
v_i	initial velocity of product formation
V_{max}	maximal reaction velocity
v_s	steady-state reaction rate in the presence of inhibitor
x	stoichiometric parameter
Z	carboxybenzyl

2. INTRODUCTION

Proteases, proteinases or peptidases are enzymes that cleave amide bonds in a polypeptide chain *via* hydrolysis (Siklos *et al.* 2015). That means that with the use of water, they degrade proteins into smaller polypeptides or single amino acids. Not only are they involved in the metabolism of ingested food, where enzymes have to be able to breakdown a wide range of substrates. Their activity is often narrowed to highly specific processes such as cell signaling, blood coagulation and fibrinolysis, or the complement system (Copeland 2005). Based on the active-site catalytic residue, they are divided into seven groups (Barrett *et al.* 2013). All enzymes of this thesis belong to the group of cysteine proteases.

Cysteine cathepsins are ubiquitously expressed in human as well as in all other living organisms, including viruses (Otto and Schirmeister 1997). Their exact function is essential for various processes and dysregulation is connected with diseases such as cancer, osteoporosis, arthritis, neurodegenerative diseases, obesity and many more (Kramer *et al.* 2017).

Rhodesain is a cathepsin L-like protease utilized by *Trypanosoma brucei rhodesiense.* This parasite is the agent causing human African trypanosomiasis, also known as sleeping sickness, which is transmitted by a bite of the vector, the tsetse fly. Not only is rhodesain required for invasion of the parasite, it is also needed for its survival (Ettari *et al.* 2016).

These proteins can serve as valuable diagnostic and therapeutic targets. Therefore, identification on new inhibitors and activity-based probes would be of great impact for the development of healthcare.

3. AIMS AND OBJECTIVES

The aim of this work is to identify and evaluate new enzyme inhibitors and activity-based probes *in vitro*. Target enzymes are human cathepsins B, K, L and S and a parasitic enzyme, rhodesain, all belonging to a group of cysteine proteases. These enzymes, involved in many serious diseases, can serve as valuable diagnostic and therapeutic targets.

In the course of this thesis, the impact of various compounds on the activity of selected enzymes will be assayed using spectrophotometric or fluorometric methods. The outcomes will then be evaluated with the use of several enzyme kinetic evaluation methods, including a visual observation of the progress curves and calculation of appropriate kinetic parameters.

Moreover, efforts will be made to identify and validate new activity-based probes, which would then serve to investigate the identity or the function of the enzyme. To prove that, sodium dodecyl sulfate polyacrylamide gel electrophoresis will be implemented.

4. Theoretical Section

4.1. Proteases

4.1.1. Definition and Classification

Proteases (proteinases, peptidases) are enzymes that cleave amide bonds in a polypeptide chain by hydrolysis (Siklos *et al.* 2015). That means a water molecule breaks down the bond and that is why they are classified among hydrolases. Proteases play a crucial role in all living organisms. By shedding, they regulate various biological processes. Besides a destructive action, as in simple digestion, they can also have an activating or deactivating function (Berg *et al.* 2015). Good examples are the blood-clotting cascade, the complement system, DNA processing or the regulation of hormones (Copeland 2005).

There are more possible ways of how to classify enzymes. According to where in the polypeptide chain the cleavage takes place, peptidases can be classified as exopeptidases or endopeptidases. Exopeptidases truncate the terminal amino acid, dipeptide or tripeptide either from the N- or C- terminus of the protein chain. These are then referred to as aminopeptidases and carboxypeptidases, respectively. On the contrary, peptidases cleaving inside the polypeptide chain are called endopeptidases (Barrett *et al.* 2013).

Based on the active-site residue of the catalytic triad, proteases are divided into cysteine, serine, threonine, aspartic, asparagine, glutamic and metallopeptidases (Barrett *et al.* 2013). These groups are then divided into clans, according to the similarities in their spatial structure, showing the evidence of sharing the evolutionary origin, or families sharing the similarity in the amino acid sequence. The MEROPS database thoroughly sorts similar peptidases into clans, characterized with two letters. The first letter represents the catalytic type (e.g. C = cysteine protease) and the second letter defines the clan. Families are characterized with the same first letter, followed by a number. All enzymes of this thesis belong to the CA clan and C1 family, of which papain is the major representative (Rawlings *et al.* 2017).

4.2. Cysteine Proteases

According to the MEROPS protease classification system, cysteine cathepsins together with rhodesain belong to the C1 family of the clan CA (Rawlings *et al.* 2017). All members of this group share a high degree of homology with papain, found in *Carica papaya* (Kamphuis *et al.* 1984), which is the representative of this group. All papain-like cathepsins are composed of two domains and display a V-shaped configuration. Besides 11 papain-like cathepsins B, C, F, H, K, L, O, S, V, W and X (Rossi *et al.* 2004), there are also four non-cysteine cathepsins encoded in the human genome, *i.e.*, cathepsins A, D, G and E (Loser and Pietzsch 2015). Cathepsins were first observed in lysosomes and were considered as intracellular enzymes, responsible for non-specific, mass proteolysis. Nowadays, it is known that they can be extracellular or intracellular, and catalyze highly specialized enzymatic reactions. However, their extra-lysosomal activity is often associated with pathological processes (Kramer *et al.* 2017). Some cathepsins are ubiquituously expressed (e.g. cathepsin B and L), whereas others show a more tissue-specific distribution. For example cathepsin K is vastly expressed in osteoclasts (Saftig *et al.* 2000) and cathepsin S in immune cells (Vidak *et al.* 2019).

4.2.1. Substrate Specificity

The active site of an enzyme has two functions. At first, it needs to bind the substrate and then to catalyze the enzymatic reaction (Ledvina *et al.* 2009). The active site of papain-like cysteine proteases contains a set of three coordinated amino acids, the so-called catalytic triad, which consists of cysteine, histidine and asparagine (Verma *et al.* 2016). However, the substrate specificity is not given just by the amino acids of the active site, but also by the specificity subsites close by. The specificity subsites (S) are pockets, which can perfectly accommodate the amino acid residues of the substrate thanks to the matching polarity, size or charge (Berger and Schechter 1970). They are numbered with respect to the distance from the active site in the polypeptide chain, primed to the site of the C-terminus and non-primed to the site of the N-terminus of the substrate. Amino

acid residues (P) of the substrate are numbered according to the corresponding subsites (Berger and Schechter 1970). The scissile bond is located between P1 and P1' of the substrate. The nomenclature is shown in **Figure 1**. The amount of binding pockets differs in various peptidases. Not even all the pockets have to be occupied.

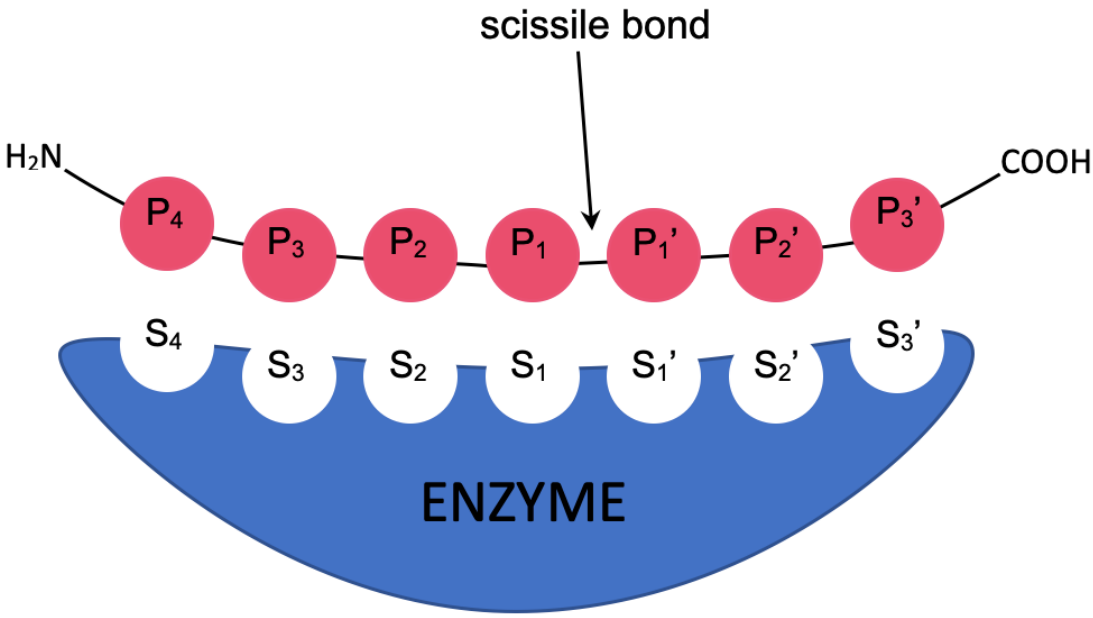

Figure 1. The nomenclature of specificity subsites and amino acid residues of the substrate according to Schechter and Berger.
S – specificity subsite; P – amino acid of the substrate

4.2.2. Catalytic Mechanism

As aforementioned, the catalytic triad of cysteine proteases consists of cysteine, histidine and asparagine. According to Lecaille *et al.* (2002), cysteine (present on the right domain) and histidine (located on the left domain) form an ion pair, which is stabilized by asparagine *via* a hydrogen bond. Histidine acts as a proton acceptor and enhances the nucleophilicity of the cysteine residue. The deprotonated cysteine residue then attacks the carbonyl carbon of the scissile bond of the substrate, forming a tetrahedral intermediate, yet reversible. A covalent bond is formed upon the release of the C-terminal portion of the substrate. The enzyme is then regenerated, when a water molecule hydrolyzes

the thioester, liberating the N-terminal portion, *via* a second tetrahedral intermediate. The corresponding mechanism is depicted in **Scheme 1**.

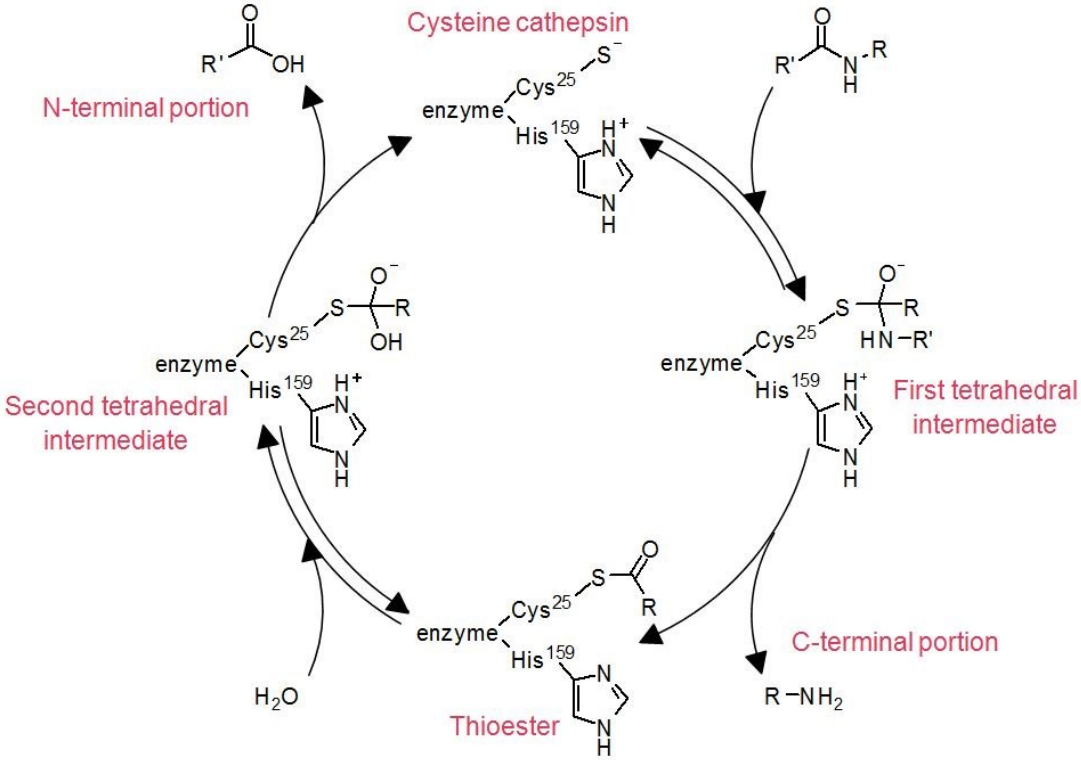

Scheme 1. Mechanism of action of cysteine proteases.
Adapted from Lecaille *et al.* (2002).

4.2.3. Endogenous Regulation

Cathepsins are vital for all living organisms, however, if their regulation is not under control, they can cause damage to our own tissues. These enzymes play a crucial role in several diseases, such as cancer, neurodegenerative diseases (Nixon *et al.* 2000), muscular dystrophy (Kar and Pearson 1978), osteoporosis, rheumathoid arthritis (Vizovisek *et al.* 2019), and many more. They can also be the cause of therapeutic resistance (Shree *et al.* 2011).

The activity of enzymes in the organism is regulated by various mechanisms. The first one is the regulation of gene expression, which means the interpretation of the information encoded in the genome. Post-translational modifications include glycosylation, S-S bridging, metal binding or proteolysis. The enzyme is usually

synthesized as a pre-proenzyme, which then needs to be altered to turn into a proenzyme, or in other words, the zymogen – an inactive form which requires to be shed to be functional. The shedding can either be catalyzed by other proteases or the zymogen is autocatalytically cleaved by the enzyme itself (López-Otín and Bond 2008). The pro-sequences not only serve as inhibitors, they can also help folding the tertiary structure of protein, stability in different pH than is optimal, and directing of a peptidase into the right place (Khan 1993).

The microenvironment of the enzyme plays a huge role. Lysosomal cathepsins require a low pH for its functioning and even stability. In a neutral environment, they would lose their activity through irreversible denaturation (Turk *et al.* (1995) and Turk *et al.* (2012)). Cysteine peptidases are also sensitive to oxidation of the cysteine in the active site. Therefore, they require reductive environment, which in cells, is accomplished by the glutathione (Giles *et al.* 2003), whereas in our experiments a reductive agent, dithithreitol (DTT) is used.

The activity of the activated enzyme can also be blocked by endogenous inhibitors. For the inhibition of cysteine cathepsins, there is a cystatin family, which is divided into subfamilies of stefins, kininogens and cystatins (Turk *et al.* 1986). Dysregulation of these inhibitors leads to a progression of a disease pathology. For example, reduced cystatin levels have been shown in late stage tumors, and on the contrary, patients with increased levels of cystatin C are at higher risk of developing cardiovascular diseases and a chronic kidney disease (Taglieri *et al.* 2009). All known endogenous inhibitors of human proteases are proteins or peptides. Another possible way of enzyme regulation is targeting to specific compartments such as lysosomes or mitochondria (Ahn and Yun 2010).

4.2.4. CATHEPSIN B

Cathepsin B is a lysosomal enzyme, which can act as both an endopeptidase and exopeptidase (dipeptidylpeptidase), depending on the surrounding pH. (Illy *et al.* 1997). This feature is accomplished by the presence of an occluding loop in the structure, that enhances the accessibility of the substrate into the active site (Illy *et al.* 1997). Elevated levels of this cathepsin have been observed in various types of cancer, such as gastric (Ebert *et al.* 2005), esophageal (Hughes *et al.* 1998), breast (Kos *et al.* 2000) or prostatic cancer (Fernandez *et al.* 2001). Cathepsin B has been shown to contribute to apoptosis as an antagonist and its absence results in increased apoptosis (Gocheva *et al.* 2006). A lack of cathepsin B also decreases angiogenesis and impairs tumor invasion (Gocheva *et al.* 2006). This cysteine protease is released in a high abundance during obesity by white adipose tissue in hypertrophied adipocytes. The activity of autophagy systems is increased and the levels of proinflammatory markers are modulated, leading to even higher macrophage infiltration. Hence, cathepsin B is found to contribute to metabolic syndrome (Araujo *et al.* 2018). The functional importance of cathepsin B is complicated by the fact that it regulates the function of related proteases. Inhibition of cathepsin B causes, for example, a deficiency of cathepsin L, which results in stimulation of cell proliferation in neoplasia (Gopinathan *et al.* 2012).

4.2.5. CATHEPSIN K

Cathepsin K is the most potent mammalian collagenase and plays a specialized role in bone resorption under both normal and pathological conditions (Barry and Platt 2012). This cathepsin is highly expressed in osteoclasts (Bromme *et al.* 1996) and secreted into the bone lacunae, the extracellular matrix, where it digests the peptidic portion of bone tissue, which is mainly made of type I collagen (Drake *et al.* 1996). Cathepsin K also has a strong elastinolytic activity (Bromme *et al.* 1996) and its overexpression is present in osteoarthritis, lung fibrosis, atherosclerosis and breast cancer (Littlewood-Evans *et al.* 1997) as well as in cervical and lung cancer (Chen and Platt 2011).

4.2.6. CATHEPSIN L

Under physiological conditions, cathepsin L is a ubiquitous, endolysosomal protease taking care of degradation of intracellular or exocyted proteins. This cathepsin is, for example, physiologically responsible for a follicular rupture during ovulation (Robker *et al.* 2000). However, in cancer, its secretion is also extended into the extracellular matrix. There, it hydrolyzes the interstitium and basal membranes, allowing the tumor to invade either locally or to metastasize into distant areas. The upregulation of cathepsin L often correlates with the tumor grade (Skrzypczak *et al.* (2012), Lah *et al.* (1997)) and can even be the key factor driving the neoplastic progression (Herszenyi *et al.* 1999). Additionally, its overexpression is present in several other human diseases, including diabetes (Huang *et al.* 2003), abdominal aortal aneurysm (Lv *et al.* 2013) or liver fibrosis (Manchanda *et al.* 2017).

4.2.7. CATHEPSIN S

Cathepsin S is an endopeptidase, which differs from many family members with the higher ability to remain active also at the neutral pH, thus has an increased potential to take part in the extracellular proteolysis (Wilkinson *et al.* 2015). The tissue expression of this cathepsin is mainly restricted to spleen and lymph, where it has been shown to be the key protease responsible for processing and degradation of autoantigens on antigen-presenting cells, such as T cells, B cells, macrophages or dendritic cells (Smith and Simons 2002). Therefore, its aberrant activity results in the induction of autoimmune diseases (Stoeckle *et al.* 2012) like bronchial asthma, rheumatoid arthritis, psoriasis, multiple sclerosis, myasthenia gravis and autoimmune diabetes (Hsing *et al.* 2010). Cathepsin S acts as a potent elastase in cardiovascular diseases such as atherosclerosis or abdominal aortic aneurysm (Jadhav *et al.* 2014). Moreover, increased levels of this protease are present in chronic renal disease (Sena *et al.* 2017). Cathepsin S is also a key contributor to nociceptive hypersensitivity in neuropathic pain (Clark *et al.* 2010). Additionally, cathepsin S plays a prominent role in cancer as well (Gocheva *et al.* 2006).

4.2.8. RHODESAIN

Rhodesain is a cathepsin L-like enzyme, which in contrast to the previous enzymes, is never present in the human body naturally. Rhodesain, synthesized by *Trypanosoma brucei rhodesiense* (*T. b. rhodesiense*), is essential for survival of this parasite and is also required to cross the blood-brain barrier of the human host (Lonsdale-Eccles and Grab 2002). *T. b. rhodesiense* is a single-cell parasite which causes African trypanosomiasis, also known as sleeping sickness, transmitted by the tsetse fly mainly in sub-Saharan Africa (Brun *et al.* 2010). When entering the host, the first, hemolymphatic stage of the disease is manifested by attacks of fever, headaches, joint pains and itching. The real danger begins with the second stage of the disease, when the parasite reaches the central nervous system. The latter stage includes a disruption of the sleep cycle, confusion, tremor, hemiparesis, etc. According to chemical evidence of Steverding *et al.* (2012), even though rhodesain is essential for the survival of *T. b. rhodesiense*, its activity must be inhibited completely to kill the parasite, otherwise it just prolongs the life of the patient.

4.3. Enzyme Inhibition

When the binding of a molecule causes a decrease in the enzyme activity or even stops the enzymatic reaction without the protein destruction, the phenomenon is called enzyme inhibition (Ledvina *et al.* 2009). This naturally occurs during cell processes to maintain homeostasis, or abnormally by undesired products of metabolism, toxins or pharmaceutical drugs. Inhibition can be distinguished as reversible or irreversible, based on the strength of the bond between the enzyme and the inhibitor.

4.3.1. Irreversible Inhibition

Irreversible inhibitors tightly bind to their target enzyme, resulting in that the inhibitor cannot dissociate from the enzyme easily (Berg et al. 2015). In general, they modify the enzyme covalently, however, in certain cases, non-covalently bound inhibitors can also remain permanently connected to the enzyme. Irreversible inhibitors usually contain a reactive functional group, *e.g.,* Michael acceptors, aldehydes or nitrogen mustards, which reacts with nucleophilic active-site amino acid residues of the enzyme (Bhatt 2001). The inhibition occurs in a time-dependent manner. In contrary to reversible inhibition, the reaction leads to a completion rather than an equilibrium. Irreversible inhibitors interact with their target in a two-step mechanism, consisting of the formation of a non-covalent complex, followed by the establishment of the covalent bond between enzyme and inhibitor (Singh *et al.* 2011). A very known example of the irreversible inhibition is acetylsalicylic acid acetylating the active-site serine of cyclooxygenase. To regain the activity, new cyclooxygenase must be synthesized (Roskoski 2008). The scheme of irreversible inhibition is shown in **Figure 2**.

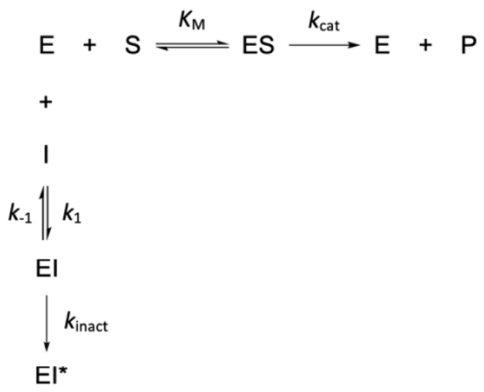

Figure 2. Scheme of irreversible inhibition.

4.3.2. REVERSIBLE INHIBITION

Reversible inhibitors form an unstable complex with the enzyme, mostly using non-covalent interactions such as hydrogen bonds, hydrophobic interactions or ionic bonds. Nevertheless, a reversible covalency can also be achieved with, for example, highly electron-deficient olefins (Senkane *et al.* 2019).

Some inhibitors can bind to the active site of the enzyme, preventing binding of the substrate, because they cannot occupy the enzyme at the same time (Bhatt 2001). Hence, they compete for the enzyme's active site and that is why this type of inhibition is called the competitive inhibition (**Figure 3a**).

In other cases, the inhibitor binds to the so-called allosteric site of the protein. An allosteric site is simply any other place than the active site, where the binding of the inhibitor causes a change in arrangement, which is no longer optimal to catalyze the enzymatic reaction (Srinivasan *et al.* 2014). This type of inhibition does not prevent the substrate from binding the enzyme, but decreases the efficiency of the enzyme (Ledvina *et al.* 2009). Since the allosteric site differs from the active site, the inhibitor binds to the enzyme alone or enzyme-substrate complex with the same affinity (Delaune and Alsayouri 2019). This type of inhibition is called the non-competitive inhibition (**Figure 3b**).

In the uncompetitive inhibition**,** the inhibitor exclusively binds to the site that becomes available only after a formation of the enzyme-substrate complex, which

causes a conformational change in the enzyme (McPherson and Pincus 2017), and precludes the product formation. This typically occurs when more substrates take part in the enzymatic reaction at the same time (Roskoski 2008) (**Figure 3c**).

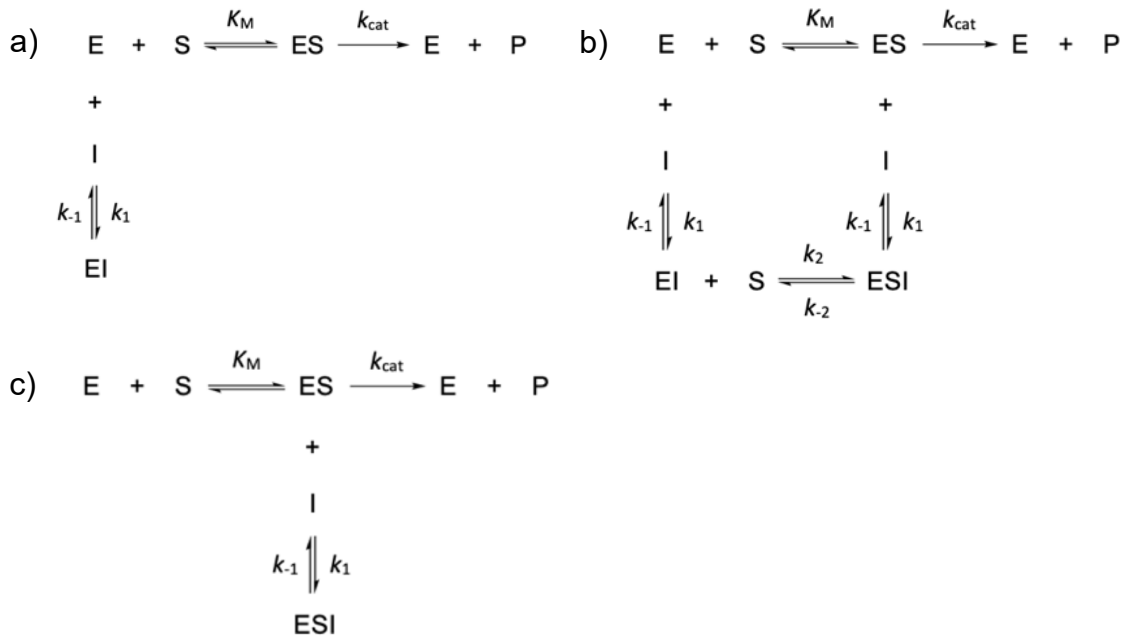

Figure 3. Schemes of reversible inhibition.
a) competitive; b) non-competitive; c) uncompetitive inhibition
E – enzyme; P – product; I – inhibitor

4.3.3. SLOW-BINDING INHIBITION

Slow-binding inhibitors can bind to the enzyme covalently or non-covalently, but always in a time-dependent manner (Silverman 2004). The enzymatic reaction is characterized by an initial burst, followed by a lower steady-state velocity. In contrary to the regular irreversible inhibition, the reaction leads to an equilibrium between the free enzyme and the enzyme-inhibitor complex instead of a completion. Unlike in classical reversible inhibition, where the equilibrium is established in milliseconds, the equilibrium in the slow-binding inhibition is established rather slowly, on a time scale of seconds to minutes (Morrison and Walsh 1988). Two possible mechanisms of the slow-binding inhibition have been proposed. The first mechanism suggests a direct, but slow binding of the inhibitor resulting in an inactivation. The second mechanism involves a rapid non-covalent binding of the inhibitor, forming an collision complex, which undergoes a slow

isomerization into the inactive enzyme-inhibitor complex (Sculley *et al.* 1996). Both possibilities are shown in **Figure 4**.

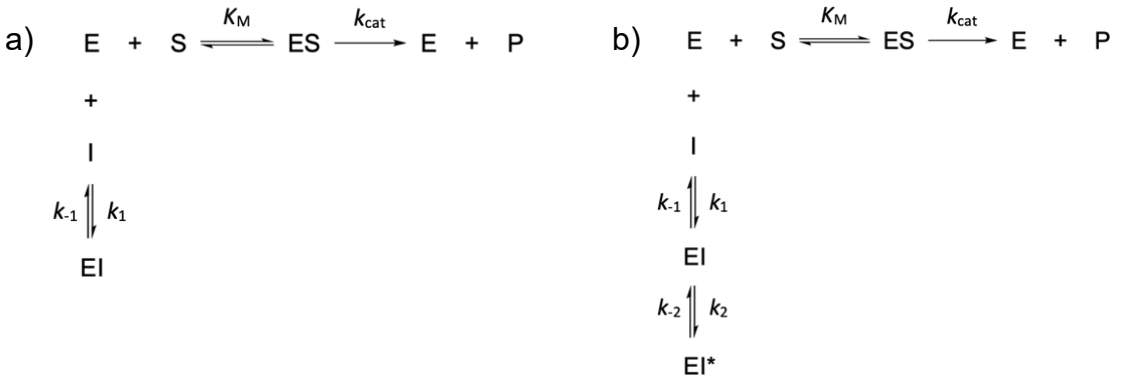

Figure 4. Two possible mechanisms of the slow-binding inhibition.
a) direct slow-binding inhibition; b) slow-binding inhibition involving the collision complex

4.4. Activity-Based Proteomics

Activity-based protein profiling (ABPP) or activity-based proteomics is a method utilizing small synthetic fluorescently or radioactively marked molecules that are designed to covalently react with the active site of the enzyme. Such molecules are called activity-based probes (ABPs). They selectively tag only active enzymes, whereas those in their inactive forms remain unlabeled. This enables to differentiate between the enzyme abundance and its elevated activity, which is regulated by a series of post-translational modifications (Serim *et al.* 2012). Protease ABPs are composed of three parts. A reactive group (warhead) covalently binds to the target enzyme. Then, there is a linker, often consisting of a peptide chain similar to the substrate, which helps to induce selectivity. Last but not least, the ABP also contains a fluorescent or radioactive reporter, allowing for a direct detection of the active enzyme (Sadaghiani *et al.* 2007). This method has emerged as a powerful proteomic strategy to identify the enzyme function in native material (Cravatt *et al.* 2008). In the course of this thesis, labeling of the enzyme is followed by gel electrophoresis and *in-gel* fluorescence scanning.

4.5. SDS-PAGE

SDS-PAGE is an electrophoresis in polyacrylamide gel in the presence of sodium dodecyl sulfate. This analytical method serves for the separation of proteins according to their molecular weight under the influence of an applied electrical field (Weber and Osborn 1969). SDS is an anionic detergent, used to mask the intrinsic net charge of proteins and to destroy their tertiary structure, resulting in the linear molecule with the negative charge, proportional to the length of the polypeptide chain. Whilst moving through the gel by application of an electric current, larger molecules are retained by the polyacrylamide gel, causing smaller molecules to migrate faster, thus further. The molecular mass can be estimated by a calculation with the relative migration distance or by comparison with a commercially available protein standard. When using a higher acrylamide concentration, the smaller mesh size gel is produced, which allows for a separation of smaller proteins.

5. EXPERIMENTAL SECTION

5.1. MATERIAL

Rhodesain was expressed and purified by Dr. Patrick Johe at the University of Mainz, Germany in the group of Prof. Dr. Tanja Schirmeister as described in (Caffrey *et al.* 2001). Cathepsin K, L and S were acquired from Enzo Life Sciences (Lörrach, Germany). Human cathepsin B and substrates (Z-Arg-Arg-pNA, Z-Phe-Arg-pNA, Z-Phe-Val-Arg-pNA, Z-Leu-Arg-AMC and Z-Phe-Arg-AMC) were purchased from Calbiochem (Merck, Darmstadt, Germany). EDTA disodium salt dihydrate was obtained from AppliChem GmbH (Darmstadt, Germany). Citric acid monohydrate, Coomassie Brilliant Blue R 250, di-sodium hydrogen phosphate dihydrate, Roti®-Nanoquant, sodium dihydrogen phosphate dihydrate, SDS, TEMED and Tris were acquired from Carl Roth GmbH + Co. KG (Karlsruhe, Germany). Acrylamide was bought from Merck (Darmstadt, Germany). Sodium chloride and methanol were obtained from Fisher Scientific U.K. Limited (Loughborough, United Kingdom). Brij 35 P was purchased from Fluka Chemie GmbH (Buchs, Switzerland). Tri-sodium citrate dihydrate and dimethylsulfoxide were purchased from Acros Organics (Geel, Belgium). Glycine was bought from Promega Corporation (Madison, USA). Acetic acid was obtained from VWR International S.A.S (Fontenay-sous-Bois, France). 2-Propanol was purchased from Rötzmeier (Salzkotten-Holsen, Germany).

5.2. INSTRUMENTS

Thermomixer Comfort, mechanical pipettes by Eppendorf (Hamburg, Germany) were used. Pipette tips sold by Sarstedt AG & Co. KG (Nümbrecht, Germany) were used. The chamber for SDS-PAGE, glass plates, buffer dam and combs were purchased from Bio-Rad (Hercules, USA). As a vortex mixer, Vortex-Genie from Scientific Industries was used. Disposable cuvettes were purchased from Brand GmbH + Co KG (Wertheim, Germany). Stirring spatula were obtained from Carl Roth GmbH + Co. KG (Karlsruhe, Germany). The spectrophotometer Cary 50 Bio by Varian (Australia) was used. For fluorometric measurements, the FLUOstar OPTIMA was acquired from BMG LABTECH GmbH (Ortenburg,

Germany). All kinetic evaluations were performed in GraFit 5.0, a data analysis software for Windows. Chemical structures were drawn in ChemDraw.

5.3. METHODS

5.3.1. DETECTION

The inhibitory potential of an enzyme inhibitor is characterized by detecting the decrease in metabolite creation by the enzyme in the presence of inhibitor. That becomes measurable when using chromogenic or fluorogenic substrates. In the course of this thesis, *para*-nitroaniline (pNA) was used as the chromogenic substrate. During the enzymatic reaction, *para*-nitroaniline is cleaved from the substrate by the enzyme, causing yellow coloring of the solution, which is measured by a UV-VIS spectrophotometer at 405 nm and expressed as the absorption per time. As a fluorometric read-out modality of the substrate consumption, 7-amino-4-methylcoumarin (AMC) was used. The emission of light (fluorescence) by released 7-amino-4-methylcoumarin is measured after excitation by the light with a wavelength of 360 nm and the emission wavelength of 440 nm on the plate reader. Examples are depicted in **Scheme 2**.

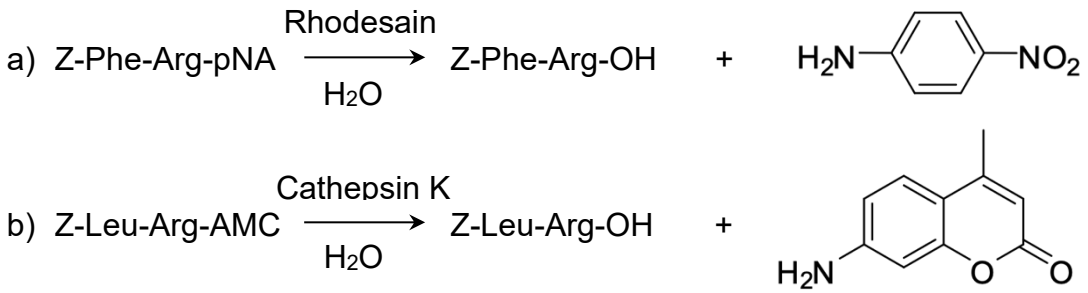

Scheme 2. Mechanism of detection.
Hydrolysis of a) chromogenic substrate by rhodesain and b) fluorogenic substrate by cathepsin K.

5.3.2. KINETIC EVALUATIONS

The inhibitory activity of substances towards an enzyme can be quantified in terms of IC_{50}, K_i or k_{inact}/K_i values. The IC_{50} value is defined as the concentration of the inhibitor at which the reaction rate is at half of the reaction rate without inhibitor (Georgakis *et al.* 2020). This constant can be calculated with the use of equation **a** in **Figure 5**. According to Sisay *et al.* (2009), in case of possible interactions in the enzymatic reaction, a stoichiometric parameter has to be applied, resulting in the so-called three-parameter equation (**Figure 5b**). The potentially time-dependent IC_{50} is a suitable way to quantify the inhibitory activity of reversible inhibitors, but may cause problems when dealing with irreversible inhibitors (Krippendorff *et al.* 2009). The inhibitory constant (K_i), in contrast to IC_{50}, is independent of the substrate concentration and the results obtained under different assay conditions are directly comparable. The K_i value can be calculated with the Cheng-Prusoff equation (**Figure 5c**), using IC_{50}, substrate concentration [S] and Michaelis-Menten value (K_M) (Cheng and Prusoff 1973).

Since covalent, thus irreversible inhibitors interact with their target in the aforementioned two-step mechanism, two parameters are important for their description. The affinity of the initial non-covalent binding is characterized by K_i and the formation of the covalent bond by the inactivation rate constant (k_{inact}) (Schmitz 2016). Together, they make up the second-order rate constant of inactivation (k_{inact}/K_i), which can be obtained by non-linear regression of first-order rate constant (k_{obs}) and inhibitor concentration [I] data pairs, using the equation **d** in **Figure 5** (Tonge 2019). According to Copeland (2005), the first-order rate constant (k_{obs}), also known as observed inhibition rate constant, describes the conversion of initial velocity of the biochemical reaction to its steady-state velocity (**Figure 5e**). When each k_{obs} is plotted *versus* its corresponding inhibitor concentration, k_{inact} can be observed as the maximum asymptote (Drawz *et al.* 2010). The concentration of the inhibitor at which the rate of inactivation is equal to half of k_{inact} is IC_{50}. K_i can be then easily calculated with the formula **c** in **Figure 5**.

Since the inhibitors with slow-binding behavior inhibit the target enzyme in a time-dependent manner, it is usually described by the inhibition constant (K_i) and, moreover, the association (k_{on}) and the dissociation constant (k_{off}) (Frizler 2012). At first, steady-state reaction rates (v_s) and the first-order rate constants (k_{obs}) have to be calculated with the slow-binding equation (**Figure 5f**) (Copeland 2005). When plotting the steady-state velocities against inhibitor concentrations and analyzing by non-linear regression (**Figure 5a**), the IC_{50} value can be acquired. Correction of IC_{50} value by the use of the Cheng-Prusoff equation (**Figure 5c**) results in the inhibitory constant (K_i). When k_{obs} is plotted *versus* inhibitor concentration [I], the apparent association constant (k_{on}') can be obtained with the equation **g** in **Figure 5**. The apparent association rate constant (k_{on}') is then corrected with the factor ($1+[S]/K_M$), according to equation **h** in **Figure 5**, resulting in the true association constant (k_{on}) (Gütschow and Neumann 1998). The true association constant is then applied in the equation **i** in **Figure 5** leading us to the dissociation constant (Schneider *et al.* 2013).

a) $$\mathrm{IC}_{50} = \frac{[\mathrm{I}]}{\frac{\mathrm{v}_0}{\mathrm{v}_\mathrm{s}} - 1}$$

b) $$\mathrm{v}_\mathrm{s} = \frac{\mathrm{v}_0}{1 + \left(\frac{[\mathrm{I}]}{\mathrm{IC}_{50}}\right)^{\mathrm{x}}}$$

c) $$K_\mathrm{i} = \frac{\mathrm{IC}_{50}}{1 + \frac{[\mathrm{S}]}{K_\mathrm{M}}}$$

d) $$k_\mathrm{obs} = \frac{k_\mathrm{inact} \times [\mathrm{I}]}{K_\mathrm{i} \times \left(1 + \frac{[\mathrm{S}]}{K_\mathrm{M}}\right) + [\mathrm{I}]}$$

e) $$[\mathrm{P}] = \frac{\mathrm{v}_\mathrm{i} \times \left(1 - \mathrm{e}^{-k_\mathrm{obs} \times \mathrm{t}}\right)}{k_\mathrm{obs}} + \mathrm{d}$$

f) $$[\mathrm{P}] = \mathrm{v}_\mathrm{s} \times \mathrm{t} + \left(\frac{(\mathrm{v}_\mathrm{i} - \mathrm{v}_\mathrm{s}) \times \left(1 - \mathrm{e}^{-k_\mathrm{obs} \times \mathrm{t}}\right)}{k_\mathrm{obs}}\right) + \mathrm{d}$$

g) $$k_\mathrm{obs} = k_\mathrm{off} + k_\mathrm{on}' \times [\mathrm{I}]$$

h) $$k_\mathrm{on} = k_\mathrm{on}' \times \left(1 + \frac{[\mathrm{S}]}{K_\mathrm{M}}\right)$$

i) $$k_\mathrm{off} = K_\mathrm{i} \times k_\mathrm{on}$$

Figure 5. General equations.

a) IC_{50} calculation (two-parameter); b) three-parameter equation; c) Cheng-Prusoff equation; d) Non-linear regression for k_{inact}; e) Exponential product formation and k_{obs} evaluation; f) Slow-binding equation; g) determination of k_{on}'; h) determination of k_{on}; i) k_{off} calculation.

[I] – inhibitor concentration; [P] – product concentration; [S] – substrate concentration; d – offset; IC_{50} – half maximal inhibitory concentration; K_i – inhibitory constant; k_{inact} – inactivation rate constant; K_M – Michaelis-Menten constant; k_{off} – dissociation constant; k_{on} – association constant; k_{on}' – apparent association constant; t – time; v_0 – reaction rate in the absence inhibitor; v_i – initial velocity of product formation; v_s – steady-state reaction rate in the presence of inhibitor; x – parameter for a reaction stoichiometry.

5.3.3. MICHAELIS-MENTEN CONSTANT

The affinity of an enzyme for a certain substrate under specific assay conditions is described by the Michaelis-Menten constant (K_M) (Ledvina *et al.* 2009). Its value is numerically equal to the concentration of the substrate at which the velocity of the enzyme reaction is half of the maximum (**Figure 6a**). The K_M value is dependent on the assay environment, such as pH, temperature or presence of effectors (Meisenberg and Simmons 2011). The lower K_M value means the higher affinity of the enzyme for the concrete substrate.

Linear plotting of the Michaelis-Menten equation helps to estimate K_M and V_{max} more accurately (Inamdar 2012). Before the non-linear curve-fitting on computers was so available, several researchers developed linearization methods of the Michaelis-Menten equation. Nowadays, computer software allows for more accurate non-linear regression methods, however, linear plotting can be useful for visualization of data (Lorsch 2014).

To review possible systematic errors, the Lineweaver-Burk and Hanes-Woolf linear plots can be performed.

a) $v_s = \frac{V_{max} \times [S]}{K_M + [S]}$

b) $\frac{[S]}{v_s} = \frac{[S]}{V_{max}} + \frac{K_M}{V_{max}}$

c) $\frac{1}{v_s} = \frac{1}{V_{max}} + \frac{K_M}{V_{max}} \times \frac{1}{[S]}$

Figure 6. a) Michaelis-Menten; b) Hanes-Woolf; c) Lineweaver-Burk equations. v_s – steady-state velocity (M s^{-1}); V_{max} – maximal reaction velocity (M s^{-1}); [S] – substrate concentration (M); K_M – Michaelis-Menten constant (M).

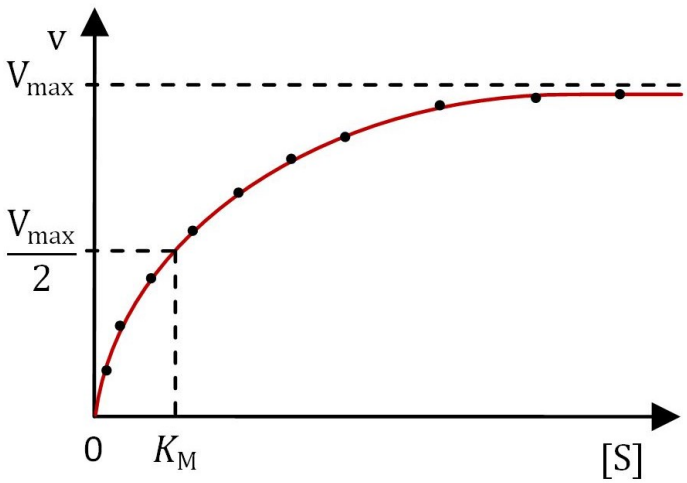

Figure 7. Michaelis-Menten plot.

The Hanes-Woolf plot, shown in **Figure 8**, is a graphical representation of the Hanes-Woolf equation (**Figure 6b**) of enzyme kinetics. The ratio of the substrate concentration and the reaction velocity is plotted against the substrate concentration (Inamdar 2012). This graphical representation is considered to be more accurate than the one of Lineweaver and Burk (Marasović *et al.* 2017).

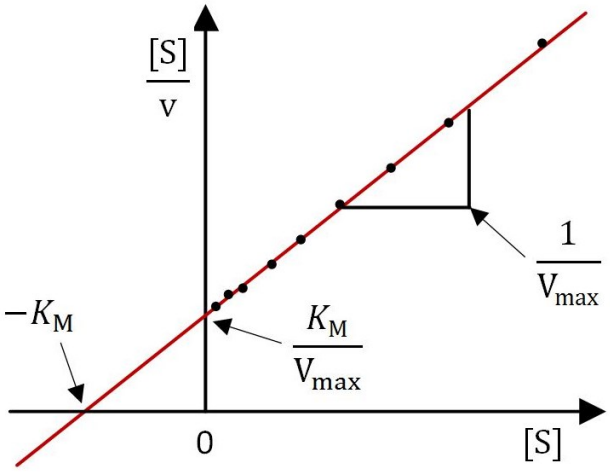

Figure 8. Hanes-Woolf plot.

The linearization method of Lineweaver-Burk plot (**Figure 9**) is a commonly used double reciprocal plot, which means that the inverse of the reaction rate is plotted against the inverse of the substrate concentration. Its equation has been described by Hans Lineweaver and Dean Burk in 1934 (**Figure 6c**). The main drawback is that the method is prone to error, since the reciprocity increases any small errors in the measurement. Additionally, the data points are not evenly distributed. Those at higher substrate concentrations are compressed into a small area, whereas the data points at lower concentrations, which are in general less accurate, affect the slope the most (Marasović *et al.* 2017).

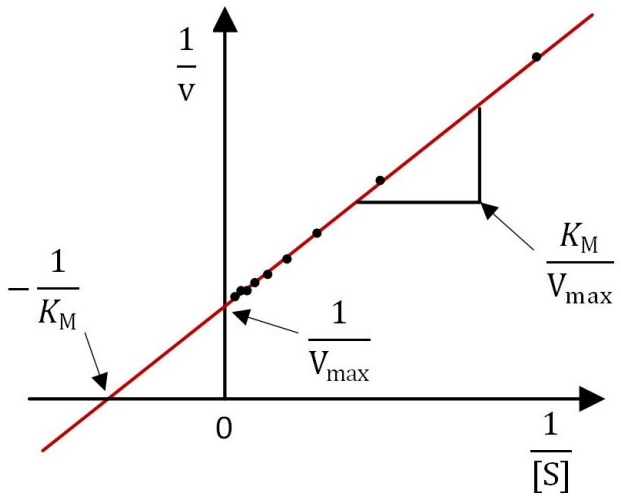

Figure 9. Lineweaver-Burk plot.

<u>Rhodesain *K*M Value Assay: UV-Photometer</u>

Rhodesain was assayed spectrophotometrically on a Cary 50 Bio, Varian at 405 nm and 25 °C in cuvettes. The enzyme (4 mg/mL in 10 mM sodium citrate buffer pH 5.0) was activated with a buffer containing 50 mM sodium acetate pH 5.5, 200 mM NaCl, 5 mM EDTA and 2 mM DTT by diluting 1:849 and was then incubated at 25 °C for 30 min. A 10 mM stock solution of the chromogenic substrate Z-Phe-Arg-pNA was prepared in DMSO. Into a cuvette containing 960 µL of the assay buffer (50 mM sodium acetate pH 5.5, 200 mM NaCl, 5 mM EDTA, 0,005% Brij 35), 10 increasing amounts of the substrate, 2% DMSO and 20 µL of the enzyme (94,1 ng/mL) were pipetted. The final substrate concentrations were 1, 2, 4, 6, 8, 10, 20, 30, 40 and 50 µM. The measurements were followed for 10 minutes in triplicate.

5.3.4. ENZYME INHIBITION ASSAYS

Rhodesain Inhibition Assay: UV-Photometer

Rhodesain was assayed spectrophotometrically on a Cary 50 Bio, Varian at 405 nm and 25 °C in cuvettes. The enzyme (4 mg/mL in 10 mM sodium citrate buffer pH 5.0) was activated with a buffer containing 50 mM sodium acetate pH 5.5, 200 mM NaCl, 5 mM EDTA and 2 mM DTT by diluting 1:850 and incubating at 25 °C for 30 min. A 10 mM stock solution of the chromogenic substrate Z-Phe-Arg-pNA was prepared in DMSO. The final substrate concentration was 40 µM (= 10.38 x K_M). The assays were performed with a final concentration of rhodesain of 23.5 ng/mL. Stock solutions of inhibitors were prepared in DMSO. The final DMSO concentration in each cuvette was 2% (20 µL). Into a cuvette containing 975 µL of the assay buffer (50 mM sodium acetate pH 5.5, 200 mM NaCl, 5 mM EDTA, 0,005% Brij 35), 4 µL of the chromogenic substrate, DMSO and inhibitor solution (16 µL) were pipetted. Upon addition of rhodesain (5 µL), the measurement was started and followed for 60 min. Adapted from (Klein *et al.* 2020)

Cathepsin B Inhibition assay: UV-photometer

Cathepsin B was assayed spectrophotometrically on a Cary 50 Bio, Varian at 405 nm and 37 °C in cuvettes, according to Frizler *et al.* (2011). The enzyme (470 µg/mL in 20 mM sodium acetate buffer pH 5.0 and 1 mM EDTA) was activated with 100 mM sodium phosphate buffer pH 6.0 containing 100 mM NaCl, 5 mM EDTA, 0.01% Brij 35 and 5 mM DTT by diluting 1:500 and incubating at 37 °C for 30 min. A 100 mM stock solution of the chromogenic substrate Z-Arg-Arg-pNA was prepared in DMSO. The final substrate concentration was 500 µM (= 0.45 × K_M). The assays were performed with a final concentration of cathepsin B of 19 ng/mL. Stock solutions of inhibitors were prepared in DMSO. The final DMSO concentration in each cuvette was 2% (20 µL). Into a cuvette containing 960 µL of the assay buffer (100 mM sodium phosphate buffer pH 6.0, 100 mM NaCl, 5 mM EDTA, 0.01% Brij 35), 5 µL of the chromogenic substrate, DMSO and inhibitor solution (15 µL) were pipetted. Upon addition of cathepsin B (20 µL), the measurement was started and followed for 60 min.

Cathepsin L Inhibition assay: UV-photometer

Cathepsin L was assayed spectrophotometrically on a Cary 50 Bio, Varian at 405 nm and 37 °C in cuvettes, according to Frizler *et al.* (2011). The enzyme (135 µg/mL in 20 mM malonate buffer pH 5.5, 400 mM NaCl and 1 mM EDTA) was activated with 100 mM sodium phosphate buffer pH 6.0 containing 100 mM NaCl and 5 mM EDTA, 0.01% Brij 35 and 5 mM DTT by diluting 1:100 and incubating at 37 °C for 30 min. A 10 mM stock solution of the chromogenic substrate Z-Phe-Arg-pNA was prepared in DMSO. The final substrate concentration was 100 µM (= 5.88 × K_M). The assays were performed with a final concentration of cathepsin L of 54 ng/mL. Stock solutions of inhibitors were prepared in DMSO. The final DMSO concentration in each cuvette was 2% (20 µL). Into a cuvette containing of the 940 µL assay buffer (100 mM sodium phosphate buffer pH 6.0, 100 mM NaCl, 5 mM EDTA, 0.01% Brij 35), 10 µL of the chromogenic substrate, DMSO and inhibitor solution (10 µL) were pipetted. Upon addition of cathepsin L (40 µL), the measurement was started and followed for 60 min.

Cathepsin K Inhibition assay: UV- photometer

Cathepsin K was assayed spectrophotometrically on a Cary 50 Bio, Varian at 405 nm and 37 °C in cuvettes, according to Frizler *et al.* (2011). The enzyme (23 µg/mL in 50 mM sodium acetate buffer pH 5.5, 50 mM NaCl, 0.5 mM EDTA, 5 mM DTT) was activated with 100 mM sodium citrate buffer pH 5.0 containing 100 mM NaCl, 1 mM EDTA, 0.01% CHAPS and 5 mM DTT by diluting 1:100 and incubating at 37 °C for 30 min. A 10 mM stock solution of the chromogenic substrate Z-Phe-Arg-pNA was prepared in DMSO. The final substrate concentration was 100 µM (= 0.85 × K_M). The assays were performed with a final concentration of cathepsin K of 54 ng/mL. Stock solutions of inhibitors were prepared in DMSO. The final DMSO concentration in each cuvette was 2% (20 µL). Into a cuvette containing of the 940 µL assay buffer (100 mM sodium phosphate buffer pH 6.0, 100 mM NaCl, 5 mM EDTA, 0.01% Brij 35), 10 µL of the chromogenic substrate, DMSO and inhibitor solution (10 µL) were pipetted. Upon addition of cathepsin K (40 µL), the measurement was started and followed for 60 min.

Cathepsin K Inhibition assay: plate reader

Cathepsin K was assayed fluorometrically on a FLUOSTAR Optima plate reader at 25 °C with an excitation wavelength of 360 nm and an emission wavelength of 440 nm on a 96 well plate, according to Frizler (2012). The enzyme (23 µg/mL in 50 mM sodium acetate pH 5.5, 50 mM NaCl, 0.5 mM EDTA, 5 mM DTT) was activated with 100 mM sodium citrate buffer pH 5.0 containing 100 mM NaCl, 1 mM EDTA 0.01% CHAPS and 5 mM DTT by diluting 1:100 and incubating at 37 °C for 30 min. A 10 mM stock solution of the fluorogenic substrate Z-Leu-Arg-AMC was prepared in DMSO. The final substrate concentration was 40 µM (= 13.33 × K_M). The assays were performed with a final concentration of cathepsin K of 4.61 ng/mL. Stock solutions of inhibitors were prepared in DMSO. The final DMSO concentration in each well was 2% (4 µL). Into a well containing 192 µL of the assay buffer (100 mM sodium citrate buffer pH 5.0, 100 mM NaCl, 1 mM EDTA and 0.01% CHAPS), 0.8 µL of the fluorogenic substrate, DMSO and inhibitor solution (3.2 µL) were pipetted. Upon addition of cathepsin K (4 µL), the measurement was started and followed for 60 min.

Cathepsin S Inhibition assay: UV- photometer

Cathepsin S was assayed spectrophotometrically on a Cary 50 Bio, Varian at 405 nm and 37 °C in cuvettes, according to Frizler *et al.* (2011). The enzyme (70 µg/mL in 199 mM MES buffer pH 6.5, 1 mM EDTA, 50 mM L-cysteine, 10 mM DTT, 0.5% Triton X-100 and 30% glycerol) was activated with 100 mM sodium phosphate buffer pH 6.0 containing 50 mM NaCl, 2 mM EDTA, 0.01% Triton X-100 and 5 mM DTT by diluting 1:100 and incubating at 37 °C for 60 min. A 10 mM stock solution of the chromogenic substrate Z-Phe-Val-Arg-pNA was prepared in DMSO. The final substrate concentration was 70 µM (= 0.58 × K_M). The assays were performed with a final concentration of cathepsin S of 28 ng/mL. Stock solutions of inhibitors were prepared in DMSO. The final DMSO concentration in each cuvette was 2% (20 µL). Into a cuvette containing 940 µL of the assay buffer (100 mM sodium phosphate buffer pH 6.0, 100 mM NaCl, 5 mM EDTA, 0.01% Brij 35), 7 µL of the chromogenic substrate, DMSO and inhibitor solution (13 µL) were pipetted. Upon addition of cathepsin S (40 µL), the measurement was started and followed for 60 min.

Cathepsin S Inhibition assay: plate reader

Cathepsin S was assayed fluorometrically on a FLUOSTAR Optima plate reader at 25 °C with an excitation wavelength of 360 nm and an emission wavelength of 440 nm on a 96 well plate, according to Mertens *et al.* (2014). The enzyme (70 µg/mL in 199 mM MES buffer pH 6.5, 1 mM EDTA, 50 mM L-cysteine, 10 mM DTT, 0.5% Triton X-100 and 30% glycerol) was activated with 100 mM sodium phosphate buffer pH 6.0 containing 100 mM NaCl, 5 mM EDTA, 0.01% Brij 35 and 5 mM DTT by diluting 1:100 and incubating at 37 °C for 60 min. A 10 mM stock solution of the fluorogenic substrate Z-Phe-Arg-AMC was prepared in DMSO. The final substrate concentration was 40 µM (= 0.74 × K_M). The assays were performed with a final concentration of cathepsin S of 42 ng/mL. Stock solutions of inhibitors were prepared in DMSO. The final DMSO concentration in each well was 2% (4 µL). Into a well containing 184 µL of the assay buffer (100 mM sodium phosphate buffer pH 6.0, 100 mM NaCl, 1 mM EDTA, 0.01% Brij 35), 0.8 µL of the fluorogenic substrate, DMSO and inhibitor solution (3.2 µL) were pipetted. Upon addition of cathepsin S (12 µL), the measurement was started and followed for 60 min.

5.3.5. SDS-PAGE

The gel is composed of two different layers, thus was cast in two steps. At first, a 12% running gel was prepared in a falcon using components as indicated below (**Table 1**) and mixed by turning upside down and back couple times. Ammonium persulfate (APS) serves as the radical initiator. After addition of tetramethylethylenediamine (TEMED), which serves as the catalyst, the solution had to be poured between the glass plates immediately. The gel solution was overlaid with isopropyl alcohol to prevent the meniscus and to protect the gel against the radical scavenger oxygen. The acrylamide had been left for polymerizing for approximately an hour. The rest of the gel solution in the falcon was used for estimating the polymerization between the glass plates. When the reaction was finished, the stacking gel solution was prepared under the same conditions and was poured in after discarding the isopropanol. A comb was immediately inserted and the gel was left polymerizing for, again, approximately an hour.

Table 1. Composition of running and stacking gels used in SDS-PAGE.

RUNNING GEL (12%)		STACKING GEL (5%)	
12 mL	30% Acrylamide	1.67 mL	30% Acrylamide
11.25 mL	Tris-buffer (pH 8.8, 1 mM)	1.25 mL	Tris-buffer (pH 6.8, 1 mM)
6.5 mL	H_2O	7 mL	H_2O
150 µL	20% SDS	50 µL	20% SDS
150 µL	10% APS	50 µL	10% APS
Mix		Mix	
24 µL	TEMED	12 µL	TEMED
Mix		Mix	

The running buffer consists of 200 mM glycine, 25 mM Tris HCl (pH 6.8), 0.1% SDS and distilled water.

ABP-Based Labeling Experiment with DTT

An amount of 4 µg of rhodesain (1 µL of the stock solution) was activated with 29 µL of the activation buffer (50 mM sodium acetate pH 5.5, 200 mM NaCl, 5 mM EDTA, 2 mM DTT) and incubated for 30 minutes at 25 °C. Decreasing amounts of the enzyme (500, 250, 200, 150, 100, 50 ng) were treated with 20 µM of the ABP, 2% of DMSO and activation buffer with total volume of 40 µL in micro-reaction vessels. One control containing 500 ng of the enzyme without the inhibitor was prepared. Solutions were incubated at 25 °C for 1 hour. After that, 8 µL of purple gel loading dye was added into each vessel, which were then subsequently denatured at 95 °C for 5 minutes. A molecular weight marker was loaded into the first gel well. Samples were carefully pipetted into their dedicated wells. Thereafter, a voltage of 120 V was applied until the loading dye reached approximately 1.5 cm from the end. The gel was then analyzed using a common gel documentation device, ChemiDoc by Bio-Rad. The assay conditions were adapted from Frizler *et al.* (2013).

ABP-Based Labeling Experiment without DTT

Decreasing amounts of rhodesain (500, 250, 200, 150, 100, 50 ng) were treated with 20 µM of the ABP and 2 µL of DMSO in the assay buffer (50 mM sodium acetate pH 5.5, 200 mM NaCl, 5 mM EDTA, 0,005% Brij 35). The control sample contained 500 ng of rhodesain, the assay buffer and 2 µL of DMSO. The total volume in each micro-reaction vessel was 12 µL. Solutions were incubated at 25 °C for 1 hour. After that, 2.4 µL of the purple gel loading dye was pipetted into each vessel and the solutions were subsequently denatured at 75 °C for 10 minutes. A molecular weight marker was loaded into the first gel well. Samples were carefully pipetted into their dedicated wells. Thereafter, a voltage of 120 V was applied until the loading dye reached approximately 1.5 cm from the end. The gel was then analyzed using a common gel documentation device, ChemiDoc by Bio-Rad. The assay conditions were adapted from Mertens *et al.* (2014).

Competition Experiment with DTT

An amount of 4 µg of rhodesain (1 µL of the stock solution) was activated with 29 µL of the activation buffer (50 mM sodium acetate pH 5.5, 200 mM NaCl, 5 mM EDTA, 2 mM DTT) and incubated at 25 °C for 30 minutes. Two dilutions of each, E-64 and ABP were prepared. Samples were prepared according to **Table 2**. A molecular weight marker was loaded into the first gel well. Samples were carefully pipetted into their dedicated wells. Thereafter, a voltage of 120 V was applied until the loading dye reached approximately 1.5 cm from the end. The gel was then analyzed using ChemiDoc by Bio-Rad. The assay conditions were adapted from Frizler *et al.* (2013).

Table 2. Pipetting scheme for the competition experiment with DTT.

	Neg. control	E-64	E-64/ABP	ABP
Assay buffer (µL)	35.45	35.45	34.65	35.45
Enzyme	500 ng /3.75 µL	500 ng /3.75 µL	500 ng /3.75 µL	500 ng /3.75 µL
DMSO (µL)	0.8	-	-	-
E-64[1]	-	0.8	-	-
E-64[2]	-	-	0.8	-
incubation at 25 °C for 10 min				
ABP[1]	-	-	-	0.8
ABP[2]	-	-	0.8	-
Incubation at 25 °C for 40 min				
Loading Dye (µL)	8	8	8	8
Denaturation at 95 °C for 5 min				

[1]Dilution 1000 µM of an inhibitor in DMSO.

[2]Dilution 1000 µM of an inhibitor in a solution of DMSO and assay buffer 1:1.

Competition Experiment without DTT

Two dilutions of each, E-64 and the ABP were prepared. Samples were prepared according to **Table 3**. A molecular weight marker was loaded into the first gel well. Samples were carefully pipetted into their dedicated wells. Thereafter, a voltage of 120 V was applied until the loading dye reached approximately 1.5 cm from the end. The gel was then analyzed using ChemiDoc by Bio-Rad. The assay conditions were adapted from Mertens *et al.* (2014)

Table 3. Pipetting scheme for the competition experiment without DTT.

	Neg. control	E-64	E-64/ABP	ABP
Assay buffer (µL)	8.75	8.75	8.75	8.75
Enzyme	500 ng/ 1.25 µL	500 ng/ 1.25 µL	500 ng/ 1.25 µL	500 ng/ 1.25 µL
DMSO (µL)	2	-	-	-
E-64[1]	-	2	-	-
E-64[2]	-	-	1	-
incubation at 25 °C for 10 min				
ABP[1]	-	-	-	2
ABP[2]	-	-	1	-
Incubation at 25 °C for 40 min				
Loading Dye (µL)	2.4	2.4	2.4	2.4
Denaturation at 95 °C for 5 min				

[1]Dilution 120 µM of an inhibitor in DMSO.

[2]Dilution 240 µM of an inhibitor in DMSO.

Selectivity of the Activity-Based Probe

Rhodesain was incubated together with or without HEK cell lysate and ABP. Four samples were prepared according to **Table 4**, each containing 200 ng of rhodesain, 2% of DMSO, assay buffer (50 mM sodium acetate pH 5.5, 200 mM NaCl, 5 mM EDTA, 0,005% Brij 35) with a total volume of 40 µL. The concentration of protein in HEK cell lysate was quantified by the Roti®-Nanoquant protein quantification assay.

Table 4. Pipetting scheme for the investigation of the selectivity of the probe.

	Neg. control	HEK cell	HEK cell/ ABP	ABP
Rhodesain (ng)	200	200	200	200
HEK cell lysate (µg)	-	4	4	-
DMSO (µL)	0.8	0.8	-	-
ABP[1]	-	-	0.8	0.8
Assay buffer (µL)	*Ad* 40	*Ad* 40	*Ad* 40	*Ad* 40
Incubation for 1 hour				
Loading dye (µL)	8	8	8	8
Denaturation at 95 °C for 5 min				

[1]1000 µM in DMSO.

5.3.6. PROTEIN QUANTIFICATION

Roti®-Nanoquant protein quantification assay was used to determine the concentration of a protein in HEK cell lysate. Roti®-Nanoquant solution (5-times conc.) had been diluted with water and 800 µL of the resulting solution was pipetted into 10 cuvettes. Different amounts of albumin (0.2-20 µg) were pipetted into 9 of them, completed with water until 1000 µL. Into the last cuvette, 2 µL of the HEK cell lysate and 198 µL of water were pipetted. A reference cuvette was

filled with 1000 µL of distilled water only (Carl Roth GmbH + Co. KG 2017). The calibration line was measured spectrophotometrically on a Cary 50 Bio, Varian at the wavelengths of 450 and 590 nm. The linearity results from the ratios of absorbances (A[590]/A[450]).

5.3.7. ANALYSIS

After the separation of proteins in SDS-PAGE is finished, those that were fluorescently labeled can be detected by a common imaging tool, ChemiDoc by Bio-Rad (Hercules, USA). This device was also used to obtain pictures.

5.3.8. COOMASSIE BLUE PROTEIN STAINING

Coomassie Brilliant Blue is an organic dye used to stain proteins by formation of stable blue complex with basic amino acids (Simpson 2010). This dye is used especially after SDS-PAGE for visualization of the protein bands on the gel. The gel is stained by incubation together with acidic staining solution under gentle agitation on a rocker at least for two hours. At first, the entire gel is dark blue, therefore a destaining solution has to be applied to wash out the abundant dye. The destaining process on a rocker takes a little longer than staining and the solution should be changed several times.

The staining solution is composed of Coomassie Brilliant Blue R (0.25 g), 100 mL of methanol, 25 mL of acetic acid and 125 mL of distilled water.

The destaining solution contains 200 mL of methanol, 50 mL of acetic acid and 200 mL of distilled water.

6. Results and Discussion

6.1. Nifedipine-Derived Compounds

The first group of compounds, which was tested in the course of this thesis, was obtained from a cooperative research group of Prof. Dr. Lhassane Ismaili from the University of Burgundy Franche-Comté, France.

Nifedipine is the first member of dihydropyridines, the calcium antagonists, which are commonly used for treating patients with hypertension (Doležal *et al.* 2016). Calcium antagonists are quite popular for prescription among doctors due to their relatively high safety and low incidence of acute side effects. Besides well-known side effects, such as swollen legs or flush in the face, all members of the group have been reported to cause gingival hyperplasia (Nishimura *et al.* 2002). The frequencies among the group vary between 19 and 38% (Steele *et al.* 1994). Not only is the overgrowth of gums an esthetic problem, but it also causes complications in possible pre-existing periodontal diseases. An inflammation of the gum can even increase the risk of cardiovascular or cerebrovascular events (Wu *et al.* 2000). Gingival hyperplasia is a result of cathepsin L inhibition as off-target. Cathepsin L is involved in the cleavage of (glyco)proteins of extracellular matrix, such as fibronectin, collagen or laminin (Ramon *et al.* 1984) and its suppression leads to the excess of the extracellular matrix in gingiva.

Besides that, a propargyl moiety on a substrate peptide or protein has been proven to react with the active-site cysteine nucleophile of target proteases, forming a vinyl thioether linkage. Interestingly, it does not react with another cysteine residues or thiol groups (Ekkebus *et al.* 2013).

To obtain the percentages of remaining enzyme activities (RA), cathepsins B and L were assayed spectrophotometrically, whereas cathepsins K and S fluorometrically. The concentration of inhibitor in tested solutions was 50 µM. The measurements were always performed in duplicates and followed for 60 minutes. The mean values of remaining enzyme activities are reported in **Table 5**. Determination of K_i values was performed in cases of RA lower than 60%.

Table 5. Enzyme inhibition by nifedipine-derived compounds.

	Structure	Remaining enzyme activity at 50 μM of inhibitor (%)			
		Cat B	Cat K	Cat L	Cat S
1	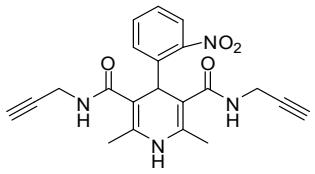	79	66	NI[a]	61
2	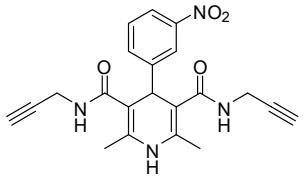	NI	72	NI	91
3	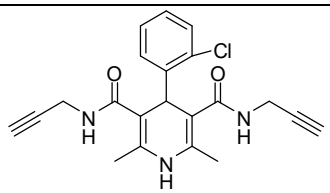	NI	85	NI	76
4	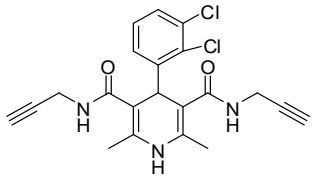	67	74	91	67
5	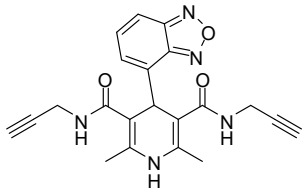	NI	62	90	77
6	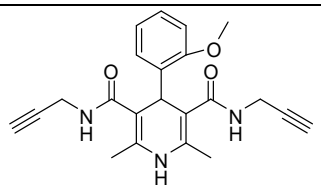	71	NI	86	67
7	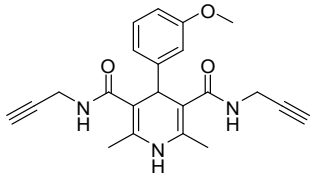	87	NI	89	67
8	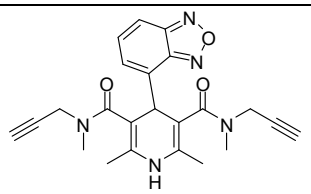	NI	73	NI	63

9	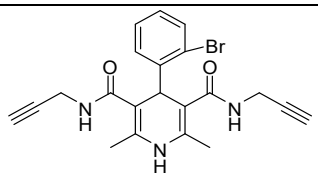	88	90	NI	70
10	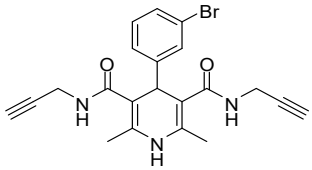	71	NI	87	54
11	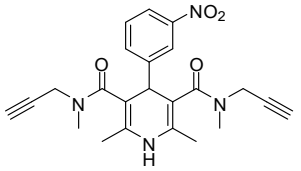	88	NI	89	74
12	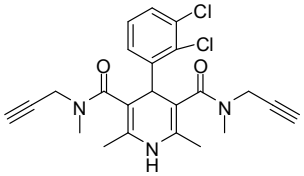	90	81	87	69
13	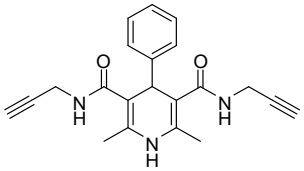	NI	NI	NI	68
14	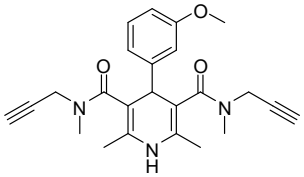	86	81	88	79
15	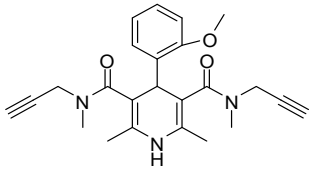	86	82	92	79
16	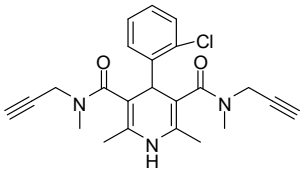	87	65	91	58
17	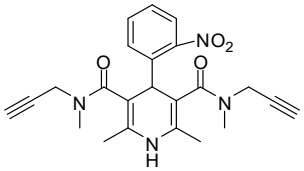	NI	83	86	70

[a]No inhibition, refers to a remaining enzyme activity higher than 95%.

Surprisingly, no inhibitors of cathepsin L were discovered. Cathepsin B and K also remained uninhibited, as well as cathepsin S in most cases. Compounds **10**

and **16** exhibited a weak inhibitory potency against cathepsin S with the remaining activities of 54% and 58%, respectively. Hence, these two compounds were further investigated in concentration dependent measurements. The progress curves are shown in **Figure 10** and **Figure 11**.

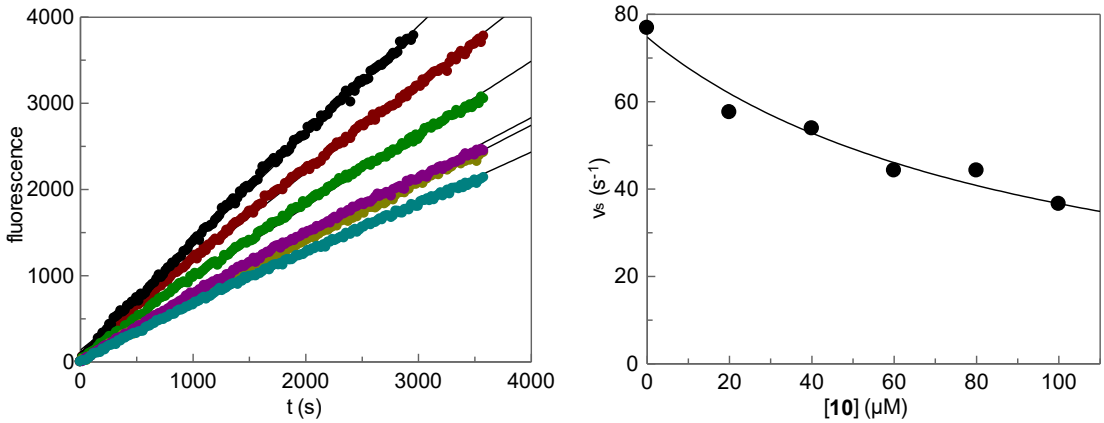

Figure 10. Inhibition of cathepsin S by **10**.

Left: Monitoring of the hydrolysis of fluorogenic substrate Z-Phe-Arg-AMC (40 μM) in the presence of increasing inhibitor concentrations (● 0 μM; ● 20 μM; ● 40 μM; ● 60 μM; ● 80 μM; ● 100 μM). Right: Plot of steady-state velocities of the substrate hydrolysis *versus* increasing concentrations of **10**. The measurements were performed in duplicates and followed for 60 minutes. Non-linear regression (**Figure 5b**) gave the IC_{50} value of 96.22 ± 12.80 μM. The K_i value of 55.30 ± 7.35 μM was calculated from the obtained IC_{50} value using the Cheng-Prusoff equation (**Figure 5c**).

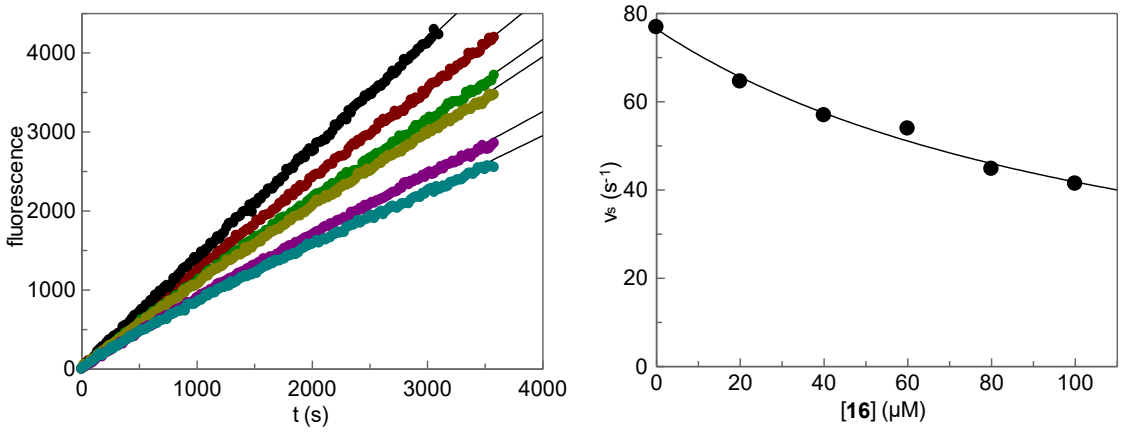

Figure 11. Inhibition of cathepsin S by **16**.

Left: Monitoring of the hydrolysis of fluorogenic substrate Z-Phe-Arg-AMC (40 μM) in the presence of increasing inhibitor concentrations (● 0 μM; ● 20 μM; ● 40 μM; ● 60 μM; ● 80 μM; ● 100 μM). Right: Plot of steady-state velocities of the substrate hydrolysis *versus* increasing concentrations of **16**. The measurements were performed in duplicates and followed for 60 minutes. Non-linear regression (**Figure 5b**) gave the IC_{50} value of 120.64 ± 9.06 μM. The K_i value of 69.33 ± 5.21 μM was calculated from the obtained IC_{50} value using the Cheng-Prusoff equation (**Figure 5c**).

The compounds **10** and **16** were found to act as weak inhibitors of cathepsin S with K_i values of 55.30 ± 7.35 and 69.33 ± 5.21 μM, respectively. Since the progress curves showed linear dependency, both substances can be considered reversible inhibitors. Besides the basic structure, which is present in the whole tested group, these two compounds do not share any similarities in the variable substituents. Hence, any structure-activity relationship cannot be deduced from the results.

6.2. CATHEPSIN K INHIBITORS AND ACTIVITY-BASED PROBES

The second series of tested compounds was synthesized for the inhibition of cathepsin K by Dominik Brajtenbach, the member of Prof. Gütschow's group. The compounds act as peptidic Michael acceptors, since they contain a vinyl sulfonamide in their structures (**Table 6**). Instead of the scissile bond of the natural substrate, there is an α,β-unsaturated amide warhead. The β-carbon is electron-poor, thus attracts the active-site cysteine for a nucleophilic attack. The substituted vinyl sulfone moiety has been proven to selectively interact with the active-site cysteine of cysteine cathepsins and remain sufficiently inert without the target (Palmer *et al.* 1995). L-leucine has been found to be favorable in P2 position of the inhibitor for the inhibition of cathepsin K and to a lesser extent also for cathepsin L and S (Bromme *et al.* 1996). In compounds **18** and **20**, the terminal amine bears *tert*-butyloxycarbonyl (Boc), which is a protecting group, stable towards most nucleophiles and bases (Felix *et al.* 2004). Compounds **19** and **21** contain cyanine-5, which is a fluorescent dye used for labeling purposes in activity-based probes (Waggoner 2006). An activity-based probe is an inhibitor which covalently binds into the catalytic site and contain a fluorescent or radioactive reporter, allowing for a direct detection of the active enzyme (Frizler 2012).

Assays were performed with four different human cathepsins, *i.e.*, B, L, K and S, and a chromogenic substrate, in the presence of compounds **18**-**21**. As anticipated, the substances exhibited the highest inhibitory potency against cathepsin K, however inhibited also the other enzymes.

The compounds were assayed using spectrophotometric methods on a Cary 50 Bio, Varian at 405 nm. For determination of remaining enzyme activity, a screening at 2.5 μM inhibitor concentration was performed. All measurements were realized in duplicates and followed for 60 minutes. The mean values of remaining enzyme activities are shown in **Table 6**.

Table 6. Remaining enzyme activity when using vinyl sulfonamide derivatives.

	Chemical structure	Remaining enzyme activity at 2.5 μM of inhibitor (%)			
		Cat B	Cat K	Cat L	Cat S
18	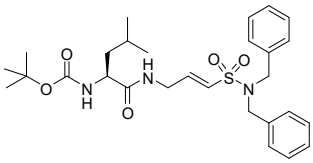	NI[a]	42	90	46
19	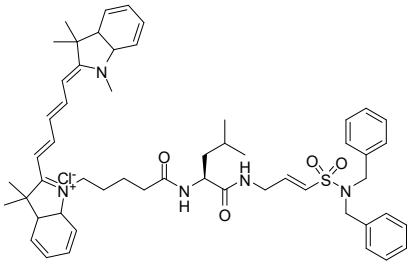	81	7	75	28
20	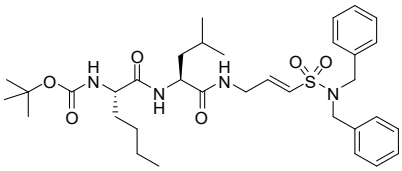	90	83	NI	66
21	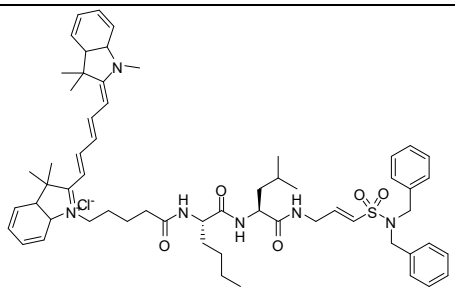	85	69	18	NI

[a]No inhibition, refers to a remaining enzyme activity higher than 95%.

Compounds which at 2.5 μM caused the remaining activity of less than 70% were further investigated. Concentration-dependent measurements were performed with 6 or 10 different concentrations of each tested compound, including the blank sample. The graphical representations of some of them are depicted in the following figures (**Figure 12-15**).

The highest inhibitory potency exhibited the activity-based probe **19** against cathpesin K with the second-order rate constant (k_{inact}/K_i) of 3 357 ± 1 232 $M^{-1}s^{-1}$, while retaining the selectivity at least 3.8-fold higher over other cathepsins. The progress curves are shown in **Figure 12**. More values together with their standard errors are reported in **Table 7**.

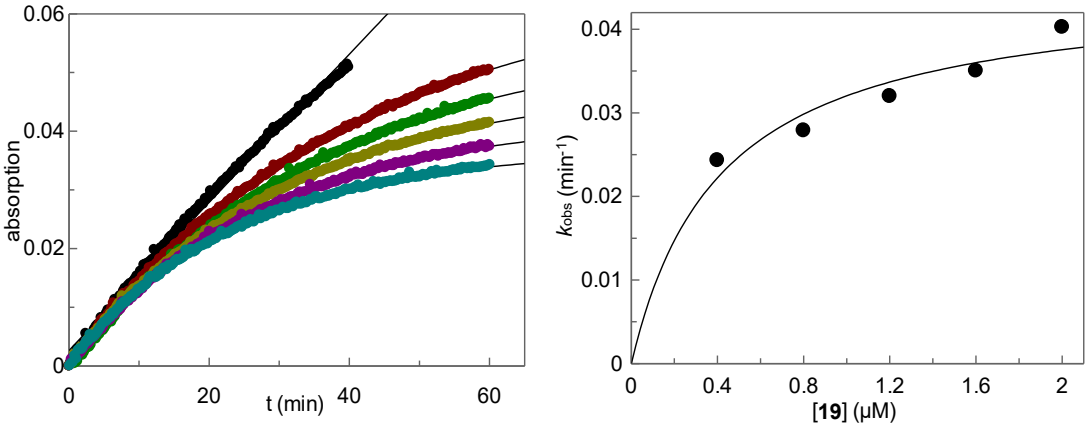

Figure 12. Inhibition of cathepsin K by **19**.

Left: Monitoring of the hydrolysis of Z-Phe-Arg-pNA (100 μM) in the presence of increasing inhibitor concentrations (● 0 μM; ● 0.4 μM; ● 0.8 μM; ● 1.2 μM; ● 1.6 μM; ● 2 μM). Right: Plot of the first-order rate constants (k_{obs}) *versus* increasing concentrations of **19**. The measurements were performed in duplicates. Non-linear regression gave the second-order rate constant (k_{inact}/K_i) of 3 357 ± 1 232 $M^{-1}s^{-1}$ according to equation **d** in **Figure 5**.

Table 7. The second-order rate constants (k_{inact}/K_i) of cathepsin K and S when inhibited by compounds **18-21**.

	k_{inact}/K_i ($M^{-1}s^{-1}$)	
	Cathepsin K	Cathepsin S
18	953 ± 258	482 ± 104
19	3 358 ± 1232	876 ± 696
20	-	188 ± 201
21	383 ± 229	-

The compound **21** caused a different type of inhibition of cathepsin L than the one observed in other cases. The progress curves showed linear dependency (**Figure 13**), *i.e.*, the inhibition is not time-dependent. Therefore, the compound can be considered a reversible inhibitor and has to be evaluated in a different manner.

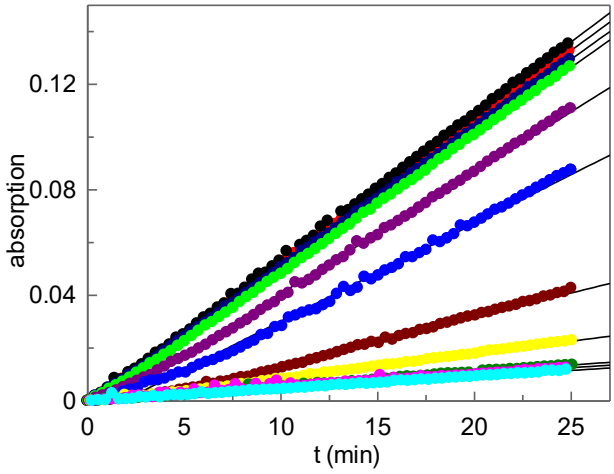

Figure 13. Inhibition of cathepsin L by **21**.

Monitoring of the hydrolysis of Z-Phe-Arg-pNA (100 μM) in the presence of 10 increasing inhibitor concentrations, including the blank sample (● 0 μM; ● 0.5 μM; ● 1 μM; ● 1.5 μM; ● 2 μM; ● 2.5 μM; ● 3 μM; ● 3.5 μM; ● 4 μM; ● 4.5 μM; ● 5 μM). The measurements were performed in duplicates and followed for 25 minutes.

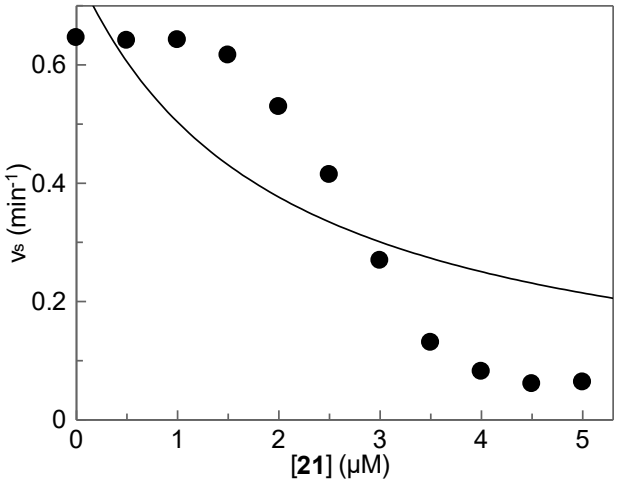

Figure 14. Plot of steady-state velocities of the substrate hydrolysis *versus* increasing concentrations of **21**, using the equation **a** in **Figure 5**.

Since the data points do not make up the typical shape of the progress curve and non-linear regression following equation **a** in **Figure 5** does not seem reasonable, there must be some interaction in the enzymatic reaction. The enzyme does not react with the substrate in a ratio of 1:1. Therefore, the stoichiometric parameter (x) has been applied into equation **a** in **Figure 5**., resulting in the so-called three-parameter equation (**Figure 5b**). The corrected plot is shown in the next figure and the results in numbers are shown in **Table 8**.

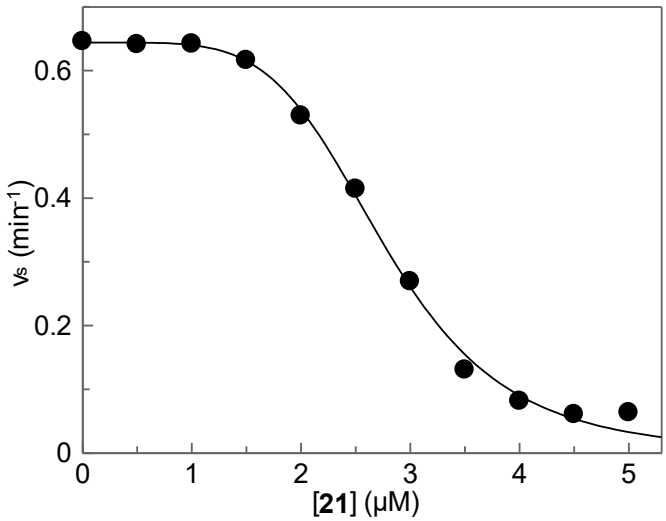

Figure 15. Corrected plot of steady-state velocities of the substrate hydrolysis *versus* increasing concentrations of **21**, using the equation **b** in **Figure 5**.

Table 8. Kinetic evaluation of **21**.

	Two-parameter model			Three-parameter model		
	IC_{50} (μM)	x	$\frac{IC_{50}}{1+\frac{[S]}{K_M}}$ (μM)	IC_{50} (μM)	x	$\frac{IC_{50}}{1+\frac{[S]}{K_M}}$ (μM)
21	1.97 ± 0.73	1	0.29 ± 0.11	2.78 ± 0.04	4.96	0.40 ± 0.01

In this series, the most significant inhibitory potency against cathepsin K exhibited compound **19**, whose progress curves were pointing to the irreversible mode of binding. Its second-order rate constant (k_{inact}/K_i) was 3 357 ± 1 232 $M^{-1}s^{-1}$ and the selectivity for cathepsin K was at least 3.8-fold higher over other cathepsins. The compound is an activity-based probe, bearing the fluorescent dye, cyanine-5, in its structure, hence could be used for labeling purposes in the future.

Moreover, the compounds containing cyanine-5 in their structure showed a greater inhibitory potency against all of the tested proteases if compared to the substances bearing *tert*-butyloxycarbonyl instead. This could indicate that cyanine-5 increases the inhibitory activity.

The measurements also revealed a distinctive behavior of the compound **21**. The reversible binding mode against cathepsin L with an unknown interaction in the enzymatic reaction has been observed. Therefore, a stoichiometric parameter has been inserted into the classical equation for IC_{50} determination (**Figure 5a**), resulting in the so-called three-parameter equation (**Figure 5b**), leading us to the IC_{50} value corrected with the factor $(1+[S]/K_M)$ of 0.40 ± 0.01 μM compared to 0.29 ± 0.11 μM, when using the simple two-parameter equation.

6.3. RHODESAIN

The enzyme gathering the most attention within this work is called rhodesain. It was expressed and purified by Dr. Patrick Johe from the group of Prof. Dr. Tanja Schirmeister at the University of Mainz in Germany, as described in Caffrey *et al.* (2001).

At first, since it had not been tested by anyone else at our institute on a spectrophotometer, the Michaelis-Menten value (K_M) has to be established for the specific assay conditions. Knowing the K_M value allows us to define possible inhibitors and their selectivity for rhodesain over other enzymes.

6.3.1. MICHAELIS-MENTEN VALUE

Caffrey *et al.* (2001) described the use of the fluorogenic substrate Z-Phe-Arg-NMec (7-amido-4-methylcoumarin) in assays with rhodesain. In the course of this thesis, the activity of rhodesain was monitored by hydrolysis of the chromogenic substrate Z-Phe-Arg-pNA in spectrophotometric assays carried on a Cary 50 Bio, Varian at 405 nm and 25 °C in cuvettes. The enzyme (4 mg/mL in 10 mM sodium citrate buffer pH 5.0) was preincubated with the activation buffer containing 50 mM sodium acetate pH 5.5, 200 mM NaCl, 5 mM EDTA and 2 mM DTT (Klein *et al.* 2020) in a dilution of 1:850 at 25 °C for 30 min. The tested solution contained 960 µL of the assay buffer consisting of 50 mM sodium acetate pH 5.5, 200 mM NaCl, 5 mM EDTA and 0,005% Brij 35 (Klein *et al.* 2020), a range of substrate concentrations between 1 and 50 µM, 2% DMSO and 20 µL of the enzyme. The measurements were followed for 10 minutes in triplicate.

The K_M value of 3.9 ± 0.6 µM was calculated with the Michaelis-Menten equation (**Figure 6a**), using means of obtained steady-state velocities plotted *versus* increasing substrate concentration. The Michaelis-Menten value was verified by using Hanes-Woolf plot. The linear regression gave the K_M value of 3.7 ± 0.6 µM. Lineweaver-Burk plot, which is more prone to error, gave the K_M value of 7.7 ± 0.9 µM, which is still not too far away from the actual result. Graphs are shown in **Figure 16**.

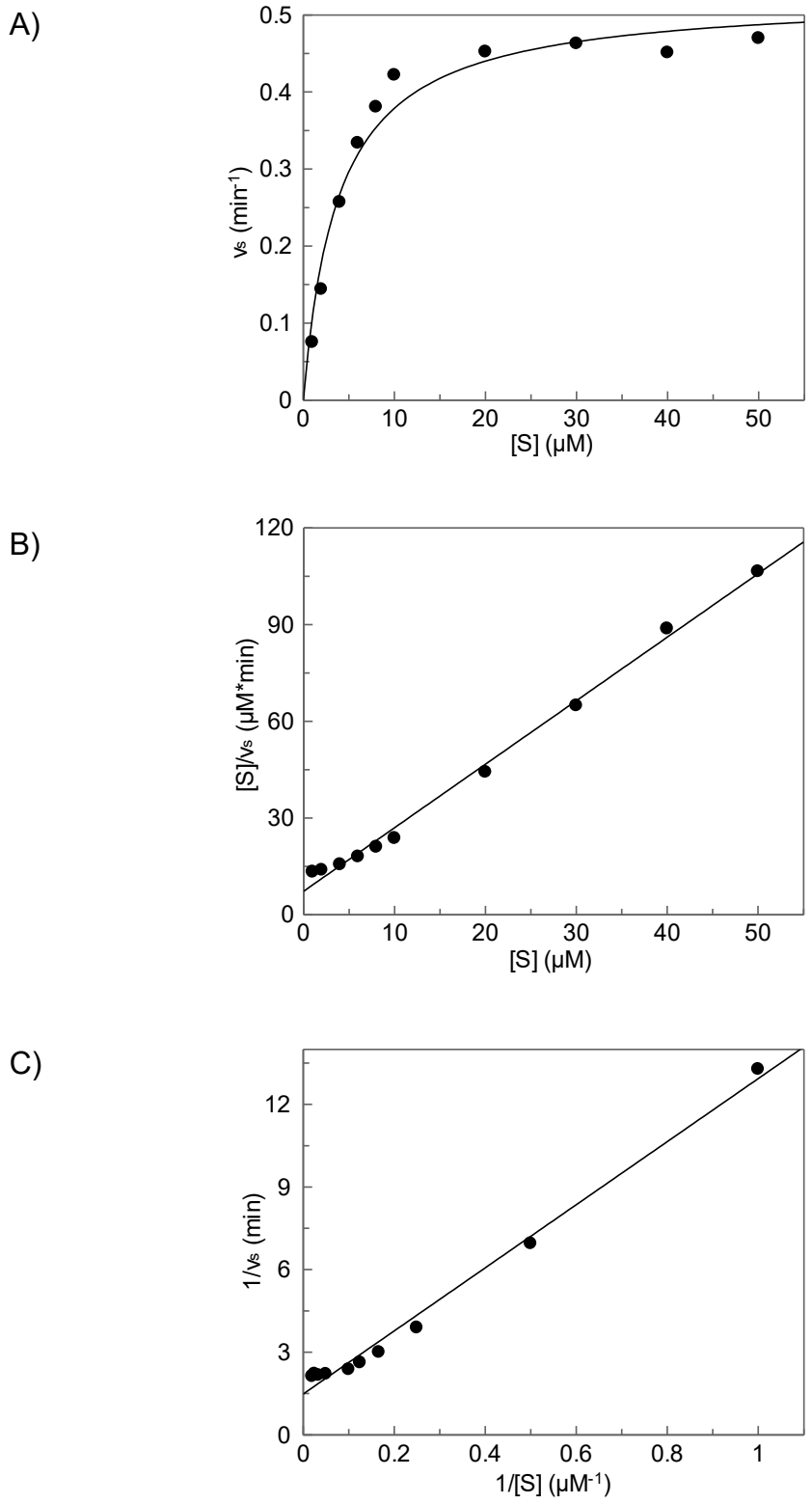

Figure 16. A) Michaelis-Menten; B) Hanes-Woolf; C) Lineweaver-Burk plot.

6.3.2. Optimization of Assay Conditions

The perfect testing solutions for the assay contain the concentration of the substrate that far exceeds the amount of the enzyme, thus the reaction rate is independent of substrate concentration (Kramer 1980). The enzyme amount is optimal when it does not consume more than 10-20% of the substrate, but it can still provide us with a sufficient read-out signal (Wu *et al.* 2003).

Several assays with various enzyme and substrate concentrations have been performed while maintaining constant amounts of other components. The solutions containing 23.5 ng (5 µL) of rhodesain and 40 µM of the substrate appear to be ideal. The concentration of DMSO is 2% and the rest is constituted by the assay buffer. The total volume in each cuvette is 1 mL.

6.3.3. Inhibition of Rhodesain by E-64

The inhibitory potency of the reference inhibitor E-64 against rhodesain was determined next to prove the appropriate and stable assay conditions. E-64 is a widely used, potent inhibitor of several cysteine proteases, which inhibits in an irreversible manner. It has been first isolated and identified from a culture of *Aspergillus japonicus* (Hanada *et al.* 1978). Since E-64 inactivates wide range of cysteine proteases, the mechanism has been extensively investigated and new inhibitors can be developed based on the structure of E-64. The structure consists of a *trans*-epoxysuccinic acid attached to a dipeptide. A common feature is a covalent bond formation between the epoxy carbon of the inhibitor and sulfur of the active-site cysteine (Varughese *et al.* 1989). The inhibition occurs *via* nucleophilic attack, which is a crucial information for uncovering the inhibitory activity (Matsumoto *et al.* 1999). Progress curves of rhodesain in the presence of different inhibitor concentrations are shown in **Figure 17**. For comparison with other enzymes, please see **Table 9**.

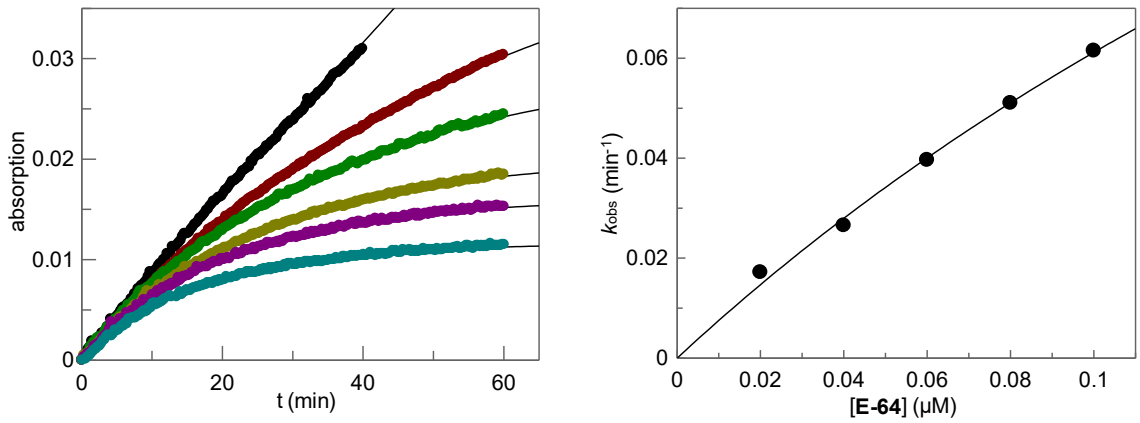

Figure 17. Inhibition of rhodesain by **E-64**.

Left: Monitoring of the hydrolysis of Z-Phe-Arg-pNA (40 μM) in the presence of increasing inhibitor concentrations (● 0 μM; ● 0.2 μM; ● 0.4 μM; ● 0.6 μM; ● 0.8 μM; ● 1 μM). Right: Plot of the first-order rate constants (k_{obs}) *versus* increasing concentrations of **E-64**. The measurements were performed in duplicates. Non-linear regression gave the second-order rate constant (k_{inact}/K_i) of 146 654 ± 82 760 $M^{-1}s^{-1}$, using the equation **d** in **Figure 5**.

Table 9. Comparison of inhibitory potency of **E-64** against selected cysteine proteases.

	Chemical structure	k_{inact}/K_i ($M^{-1}s^{-1}$)				
		Cat B	Cat K	Cat L	Cat S	Rhod
E-64	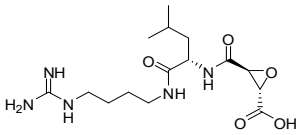	258 009 ± 61 917[a]	192 194 ± 101 750[a]	98 073 ± 60 441[a]	142 483 ± 53 967[a]	146 654 ± 82 760

[a]Measurements and the kinetic evaluation were performed by Carina Lemke.

As expected, rhodesain is inhibited as well as other cysteine proteases because E-64 is a pan-cysteine protease inhibitor.

6.3.4. Screening of a Small Compound Library as Potential Inhibitors for Rhodesain

A small library of compounds was tested for rhodesain inhibition, all bearing a thiophene moiety directly attached to a heterocyclic system, in order to find new potential lead compounds for the discovery of rhodesain inhibitors. Spectrophotometrical assays were performed with 5 µM of the potential inhibitor. The measurements were followed for 60 minutes. Unfortunately, none of them has shown significant inhibition. Moreover, compounds **34** and **37** were even very poorly soluble under testing conditions, resulting in precipitation. When using lower concentration (3 µM), no inhibition was observed. Structures of the compounds and means of the remaining enzyme activities from duplicate measurements are reported in **Table 10**.

Table 10. Inhibition of rhodesain by heterocyclic compounds.

	Chemical structure	Remaining enzyme activity at 5 µM of inhibitor (%)
22	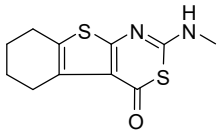	NI[a]
23	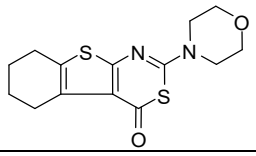	NI
24	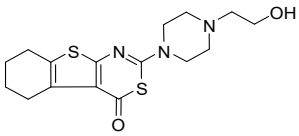	91
25	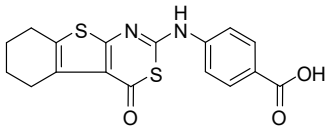	NI
26	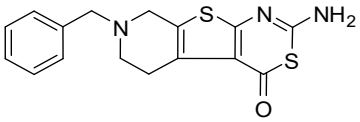	90
27	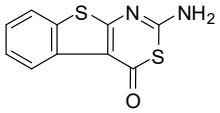	NI

28	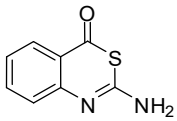	NI
29	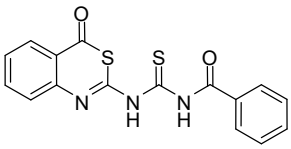	NI[b]
30	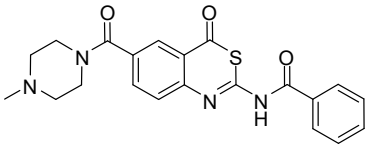	92
31	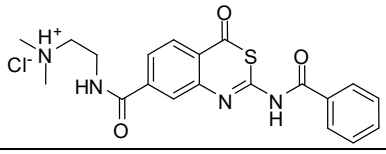	76
32	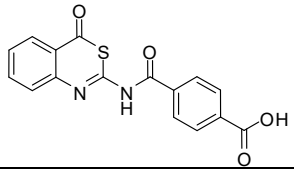	NI[b]
33	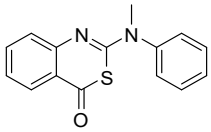	74
34	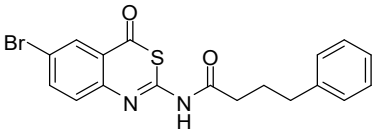	89
35	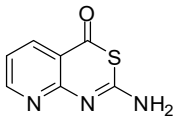	NI

[a]No inhibition, refers to a remaining enzyme activity higher than 95%.

[b]Precipitated at 5 μM, thus measured at 3 μM.

6.3.5. INHIBITION OF RHODESAIN BY PHENYL VINYL SULFONES

The following substances were synthesized for rhodesain by Carina Lemke and Dr. Matthias Dieter Mertens. The structures always contain a peptidic backbone with an electrophilic phenyl vinyl sulfone warhead, which acts as the Michael acceptor and selectively interacts with the active-site cysteine of cysteine cathepsins. Compound **36** bears a phenylalanine moiety in P2 position, proven to be beneficial for rhodesain inhibition (Giroud *et al.* 2018). To increase selectivity towards rhodesain, compounds **37** and **38** incorporate *meta* and *para*-substitutions at the phenyl ring of the P2 amino acid (Jaishankar *et al.* 2008). In compounds **36-38,** the terminal amine of the phenylalanine bears *tert*-butyloxycarbonyl (Boc), which is a protecting group, stable towards most nucleophiles and bases (Felix *et al.* 2004), whereas in compounds **39** and **40,** there is a fluorophore, making them potential activity-based probes. Chemical structures and results in numbers are summarized in **Table 11**.

Table 11. Kinetic evaluation of inhibitory potency of **36**-**40**.

	Chemical structure	k_{inact}/K_i ($M^{-1}s^{-1}$)				
		Cat B	Cat K	Cat L	Cat S	Rhod
36	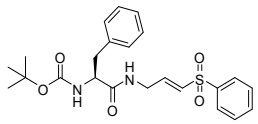	378 ± 12[a]	1 324 ± 473[a]	5 884 ± 681[a]	7 960 ± 4 413[a]	135 948 ± 87 605
37	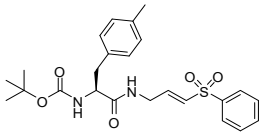	161 ± 30.6	445 ± 188	5 844 ± 10 929	15 461 ± 2 761	74 662 ± 147 418
38	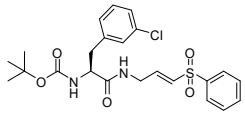	580 ± 166	954 ± 459	16 387 ± 1 395	21 257 ± 3 899	75 207 ± 131 918
39	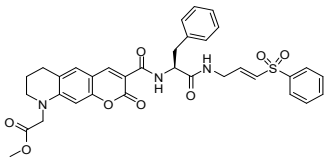	90.3 ± 33.9[b]	886 ± 376[b]	405 ± 69[b]	362 ± 65[b]	3 405 ± 832[c]
40	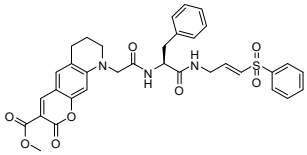	364 ± 65[b]	6 239 ± 5 240[b]	19 858 ± 3 294[b]	43 258 ± 26 343[b]	26 102 ± 7 495

Cat – cathepsin; Rhod – rhodesain

[a]Measurements were performed by Dr. Janina Schmitz and evaluated by Duyen Dao.

[b]Measurements and the kinetic evaluation were performed by Carina Lemke.

[c]**39** behaved as a slow-binding inhibitor, evaluation was performed according to equations **f-i** in **Figure 5**.

The greatest inhibitory potency against rhodesain exhibited peptidomimetic inhibitor **36**, containing unsubstituted phenyl of phenylalanine and Boc protecting group. Its second-order rate constant was 135 948 ± 87 605 $M^{-1}s^{-1}$ according to equation **d** in **Figure 5**, which is nearly equal to the (k_{inact}/K_i) of reference inhibitor **E-64** (146 654 ± 82 760 $M^{-1}s^{-1}$). The selectivity of **36** for rhodesain was at least 17-fold higher over other cathepsins.

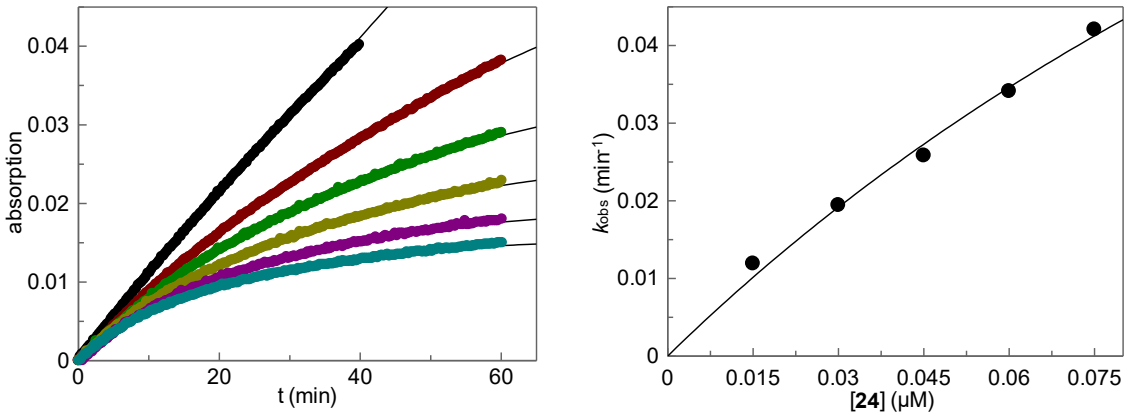

Figure 18. Inhibition of rhodesain by **36**.
Left: Monitoring of the hydrolysis of Z-Phe-Arg-pNA (40 μM) in the presence of increasing inhibitor concentrations (● 0 μM; ● 0.015 μM; ● 0.03 μM; ● 0.045 μM; ● 0.06 μM; ● 0.075 μM). Right: Plot of the first-order rate constants (k_{obs}) *versus* increasing concentrations of **36**. The measurements were performed in duplicates. Non-linear regression gave the second-order rate constant (k_{inact}/K_i) of 135 948 ± 87 605 $M^{-1}s^{-1}$ according to equation **d** in **Figure 5**.

Two derivatives of the previous compound with substitutions on the phenyl ring of the phenylalanine in P2 position were tested on rhodesain and other enzymes. Compound **37** contains a methyl group in *para* position and the compound **38** offers chlorine in *meta* position. Both of them have shown a significant inhibitory potency against rhodesain, however, compound **37** exhibited a higher selectivity. The second-order rate constants (k_{inact}/K_i) are 74 662 ± 147 418 $M^{-1}s^{-1}$ and 75 207 ± 131 918 $M^{-1}s^{-1}$ for compounds **37** and **38**, respectively. Higher errors are caused by the use of inhibitor concentrations, which are way lower than the inhibitory constant. When plotting the first-order rate constants (k_{obs}) *versus* increasing concentrations of the inhibitor, the curve is flatter (e.g., **Figure 19** and **Figure 22**), and therefore, the second-order rate constant is more difficult to

estimate, resulting in a reduced accuracy. The selectivity of **37** for rhodesain is 4.8 times higher over other cathepsins, whereas the one of **38** just 3.5 times. The values could indicate, that the substitution on the phenylalanine causes decrease in inhibitory potency, however, the remaining enzyme activities of rhodesain, if inhibited by compounds **37** and **38** at a concentration of 10 μM, were little lower than the RA in case of compound **36**, even though they were all around 0. Progress curves of the activity of various enzymes when using the compound **37** are depicted the following figures (**19-23**).

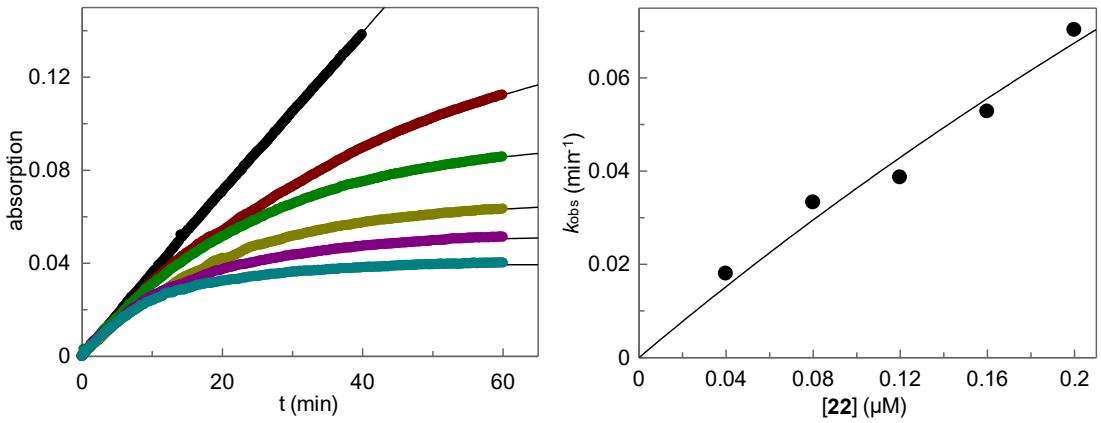

Figure 19. Inhibition of rhodesain by **37**.

Left: Monitoring of the hydrolysis of Z-Phe-Arg-pNA (40 μM) in the presence of increasing inhibitor concentrations (● 0 μM; ● 0.04 μM; ● 0.08 μM; ● 0.12 μM; ● 0.16 μM; ● 0.2 μM). Right: Plot of the first-order rate constants (k_{obs}) *versus* increasing concentrations of **37**. The measurements were performed in duplicates. Non-linear regression gave the second-order rate constant (k_{inact}/K_i) of 74 662 ± 147 418 $M^{-1}s^{-1}$, using the equation **d** in **Figure 5**.

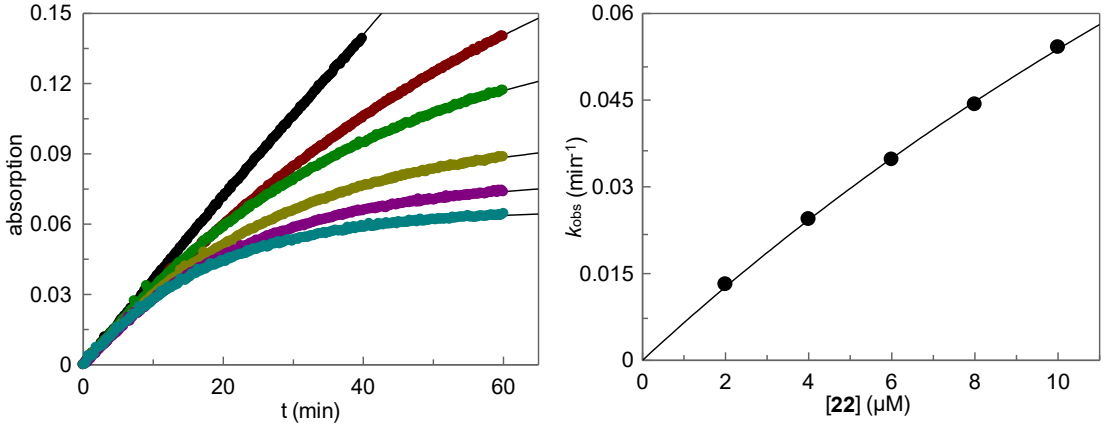

Figure 20. Inhibition of cathepsin B by **37**.

Left: Monitoring of the hydrolysis of Z-Arg-Arg-pNA (500 μM) in the presence of increasing inhibitor concentrations (● 0 μM; ● 2 μM; ● 4 μM; ● 6 μM; ● 8 μM; ● 10 μM). Right: Plot of the first-order rate constants (k_{obs}) *versus* increasing concentrations of **37**. The measurements were performed in duplicates. Non-linear regression gave the second-order rate constant (k_{inact}/K_i) of 160.54 ± 30.63 $M^{-1}s^{-1}$, using the equation **d** in **Figure 5**.

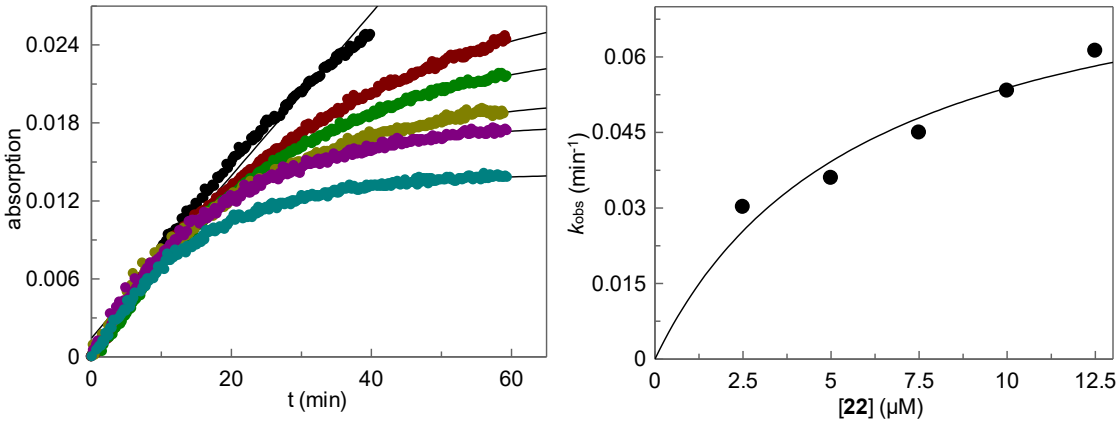

Figure 21. Inhibition of cathepsin K by **37**.

Left: Monitoring of the hydrolysis of Z-Phe-Arg-pNA (100 μM) in the presence of increasing inhibitor concentrations: (● 0 μM; ● 2.5 μM; ● 5 μM; ● 7.5 μM; ● 10 μM; ● 12.5 μM). Right: Plot of the first-order rate constants (k_{obs}) *versus* increasing concentrations of **37**. The measurements were performed in duplicates. Non-linear regression gave the second-order rate constant (k_{inact}/K_i) of 445.12 ± 187.63 $M^{-1}s^{-1}$, using the equation **d** in **Figure 5**.

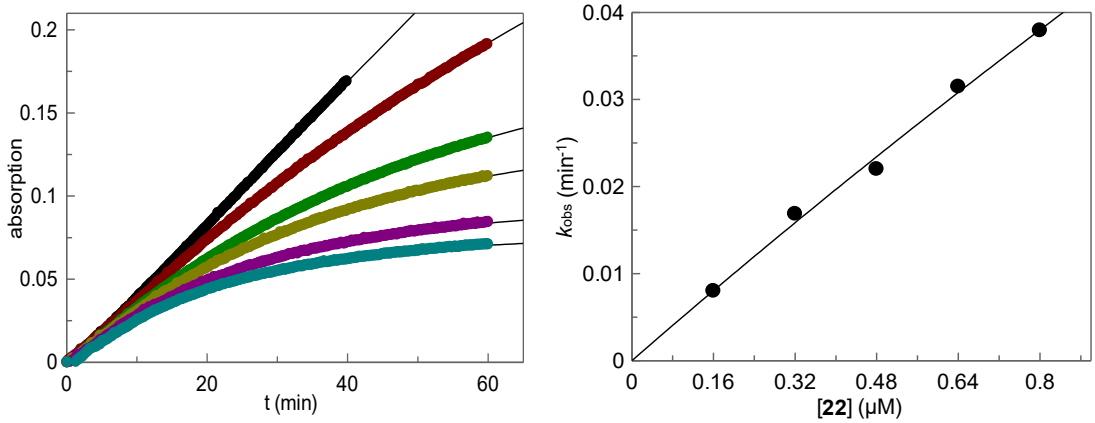

Figure 22. Inhibition of cathepsin L by **37**.

Left: Monitoring of the hydrolysis of Z-Phe-Arg-pNA (100 μM) in the presence of increasing inhibitor concentrations: (● 0 μM; ● 0.16 μM; ● 0.32 μM; ● 0.48 μM; ● 0.64 μM; ● 0.8 μM). Right: Plot of the first-order rate constants (k_{obs}) *versus* increasing concentrations of **37**. The measurements were performed in duplicates. Non-linear regression gave the second-order rate constant (k_{inact}/K_i) of 5 844 ± 10 929 $M^{-1}s^{-1}$, using the equation **d** in **Figure 5**.

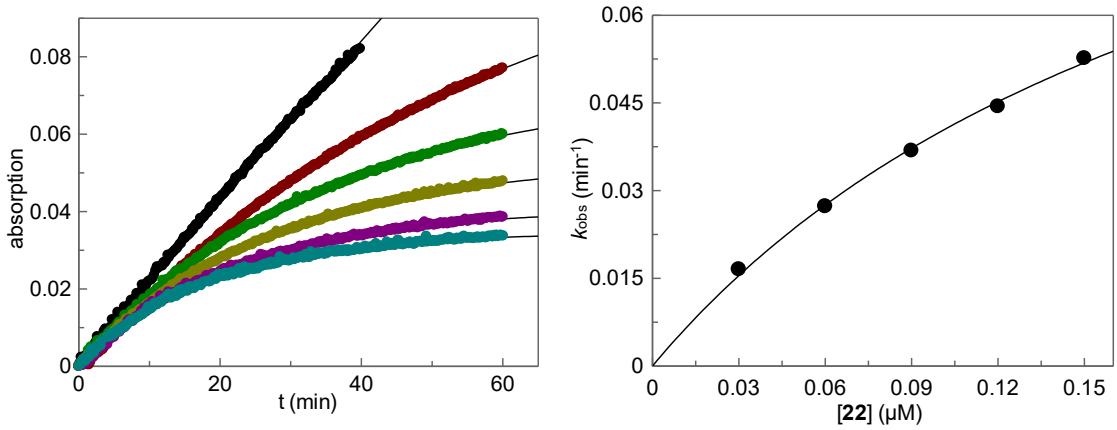

Figure 23. Inhibition of cathepsin S by **37**.

Left: Monitoring of the hydrolysis of Z-Phe-Val-Arg-pNA (70 μM) in the presence of increasing inhibitor concentrations (● 0 μM; ● 0.3 μM; ● 0.6 μM; ● 0.9 μM; ● 1.2 μM; ● 1.5 μM). Right: Plot of the first-order rate constants (k_{obs}) *versus* increasing concentrations of **37**. The measurements were performed in duplicates. Non-linear regression gave the second-order rate constant (k_{inact}/K_i) of 15 461 ± 2 761 $M^{-1}s^{-1}$, using the equation **d** in **Figure 5**.

Compounds **39** and **40** are potential activity-based probes with the unsubstituted phenylalanine and coumarin as the fluorophore in their structure. The analysis of the inhibition mode of compound **39** has clearly revealed the slow-binding behavior (seen in **Figure 24**), which is characterized by an initial exponential phase, followed by a linear steady-state equilibrium. This is hardly explainable, since Michael acceptors are prone to undergo irreversible inhibition. This type of time-dependent inhibition needs to be evaluated in a different manner, described by the association (k_{on}) and the dissociation constant (k_{off}), in addition to the inhibition constant (K_i). Results obtained using equations **f-i** in **Figure 5** are shown in **Table 12**. Due to the non-complete irreversibility, compound **39** is not the preferred candidate for activity-based probing, in contrast to **40**, which seems to inhibit rhodesain with full irreversibility. Compound **40** acts as a reasonable inhibitor of rhodesain. Non-linear regression gave the second-order rate constant (k_{inact}/K_i) of 26 102 ± 7 495 $M^{-1}s^{-1}$, according to equation **d** in **Figure 5**. With regard to different inhibition modes of these two compounds, their inhibitory potency is not directly comparable. Nevertheless, remaining enzyme activity of rhodesain in a solution with 10 μM of inhibitor was 20% in case of compound **39** and 0% for **40**. Although compound **40** was not very selective for rhodesain, and cathepsin S was even better inhibited, this probe was a satisfactory starting point for in-gel detection of rhodesain.

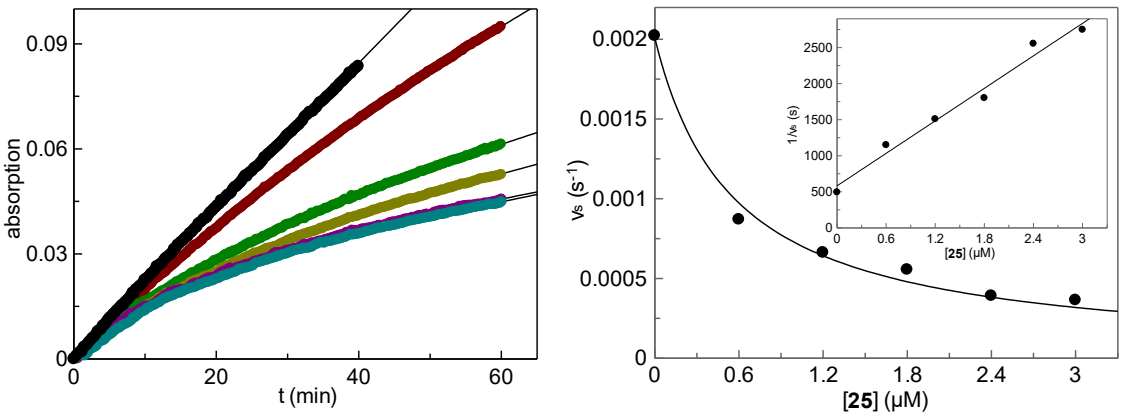

Figure 24. Inhibition of rhodesain by **39**.

Left: Monitoring of the hydrolysis of Z-Phe-Arg-pNA (40 μM) in the presence of increasing inhibitor concentrations (● 0 μM; ● 0.6 μM; ● 1.2 μM; ● 1.8 μM; ● 2.4 μM; ● 3 μM). Right: Plot of steady-state velocities *versus* increasing concentrations of **39**. The insert is a Dixon plot showing a linearity.

Table 12. Kinetic evaluation of slow-binding behavior of **39**.

	k_{on} ($M^{-1}s^{-1}$)	k_{off} ($10^{-4}s^{-1}$)	K_i (nM)
39	2 922.21	1.45	49.62

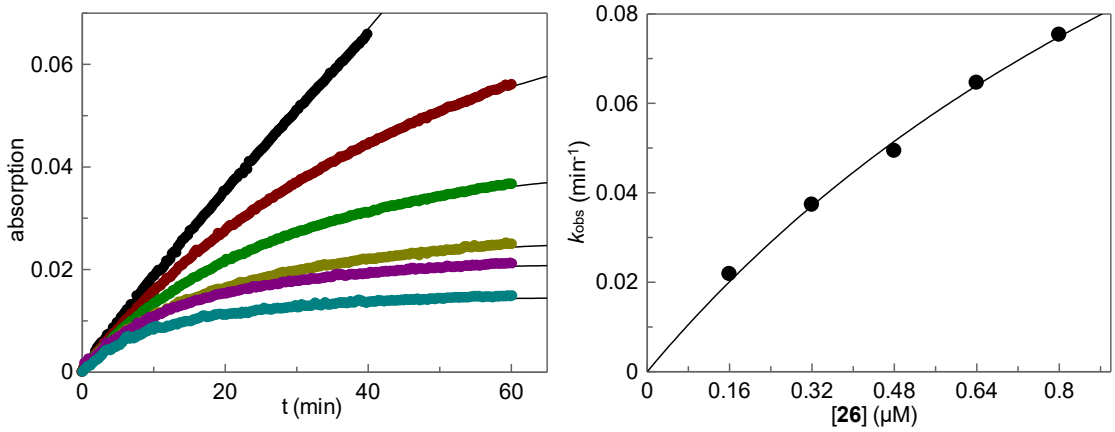

Figure 25. Inhibition of rhodesain by **40**.

Left: Monitoring of the hydrolysis of Z-Phe-Arg-pNA (40 μM) in the presence of increasing inhibitor concentrations (● 0 μM; ● 0.16 μM; ● 0.32 μM; ● 0.48 μM; ● 0.64 μM; ● 0.8 μM). Right: Plot of the first-order rate constants (k_{obs}) *versus* increasing concentrations of **40**. The measurements were performed in duplicates. Non-linear regression gave the second-order rate constant (k_{inact}/K_i) of 26 102 ± 7 495 $M^{-1}s^{-1}$, according to equation **d** in **Figure 5**.

6.3.6. PROBE APPLICATION IN SDS-PAGE ANALYSIS

Since the compound **40** has shown a significant inhibitory potency against rhodesain and contains a fluorophore in its structure, it was then further investigated in SDS-PAGE analysis. Compound **39** possesses the fluorophore as well, but the inhibition of rhodesain was not as potent nor convenient. The purpose of these assays was to show the selectivity of labeling by the probe, which could then be used for a protein identification and profiling.

Initially, to identify the enzyme in the gel and find its ideal concentration, the electrophoresis with various concentrations of the enzyme was performed.

In the first experiment, rhodesain was incubated with the activation buffer, containing 50 mM sodium acetate pH 5.5, 200 mM NaCl, 5 mM EDTA and 2 mM DTT for 30 minutes at 25 °C. Decreasing amounts of the enzyme (500, 250, 200, 150, 100, 50 ng) were treated with 20 µM of **40**, 2% of DMSO and activation buffer with total volume of 40 µL in micro-reaction vessels. Solutions were incubated at 25 °C for 1 hour. After that, 8 µL of purple gel loading dye was added into each vessel and subsequently denatured at 95 °C for 5 minutes. The blank sample (C) containing just the enzyme (500 ng) and no probe, but has been processed parallelly with other samples, serves as a control to confirm the efficiency of the labeling (Galmozzi *et al.* 2014). A molecular weight marker was loaded into the first gel well. Samples were carefully pipetted into their dedicated wells. Thereafter, a voltage of 120 V was applied until the loading dye reached approximately 1.5 cm from the end. The gel was then analyzed using a common gel documentation device, ChemiDoc by Bio-Rad, and after that stained with the Coomassie Blue staining solution (**Figure 26**). The assay conditions were adapted from Frizler *et al.* (2013).

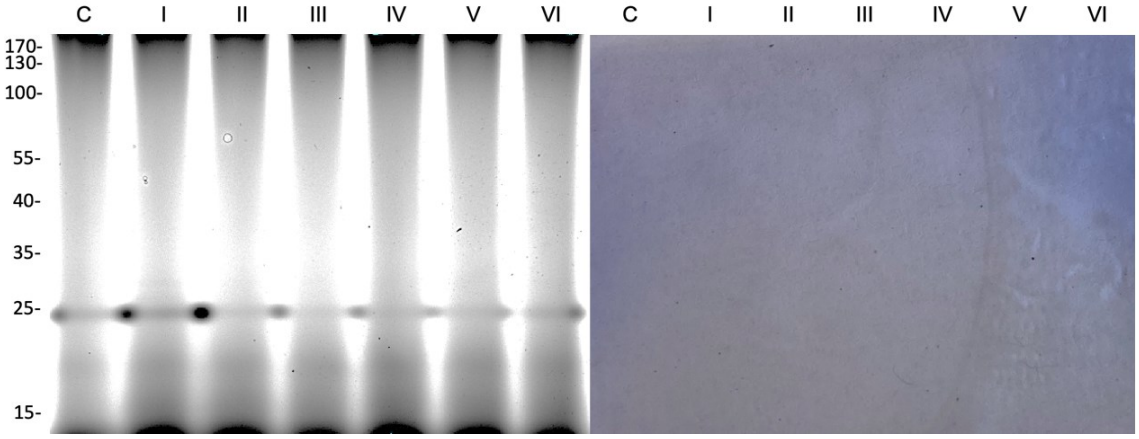

Figure 26. SDS-PAGE with decreasing concentrations of rhodesain and DTT. Left: ChemiDoc detection image, excitation wavelenght 485 nm, emission wavelenght 515 nm. Right: Coomassie Blue staining.
C – 500 ng; I – 500 ng; II – 250 ng; III – 200 ng; IV – 150 ng; V – 100 ng; VI – 50 ng of rhodesain, which was preincubated with the activation buffer. All samples except the first, control sample, contain an abundant amount (20 µM) of compound **40**.

With the use of this method, successful labeling could not be detected besides an unknown band, which was present over the entire width of the gel. The gel was additionally stained with Coomassie Blue and neither then anything could be seen.

The concentration assay was repeated with different assay conditions, adapted from Mertens *et al.* (2014). The enzyme was not treated with the activation buffer, whereas directly pipetted into micro-reaction vessels containing the assay buffer (50 mM sodium acetate pH 5.5, 200 mM NaCl, 5 mM EDTA, 0,005% Brij 35), 20 µM of compound **40** and 2 µL of DMSO, with the total volume of 12 µL. Solutions were incubated at 25 °C for 1 hour. After that, 2.4 µL of the purple gel loading dye was pipetted into each vessel and the solutions were subsequently denatured at 75 °C for 10 minutes. A molecular weight marker was loaded into the first gel well. Samples were carefully pipetted into their dedicated wells. Thereafter, a voltage of 120 V was applied until the loading dye reached approximately 1.5 cm from the end. The gel was then analyzed using a common gel documentation device,

ChemiDoc by Bio-Rad, and after that stained with the Coomassie Blue staining solution (**Figure 27**).

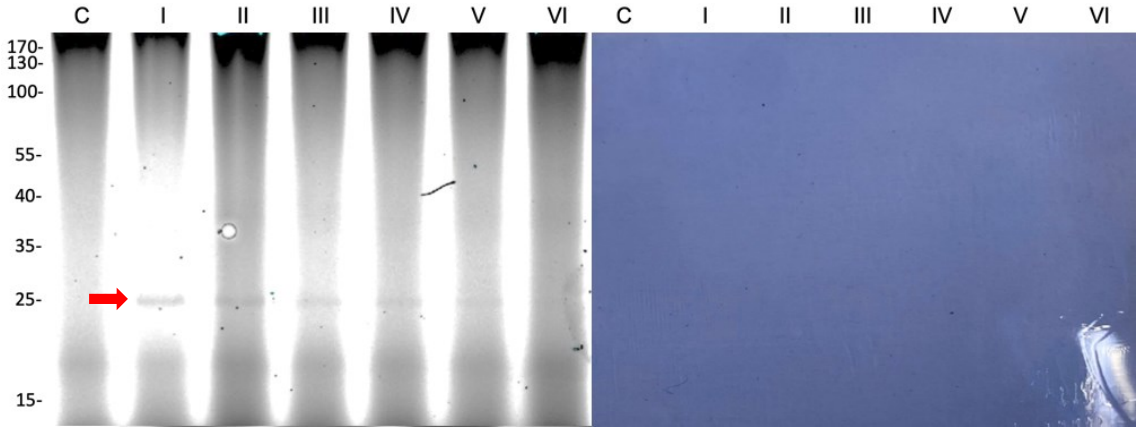

Figure 27. SDS-PAGE with decreasing concentrations of the enzyme.
Left: ChemiDoc detection image, excitation wavelenght 485 nm, emission wavelenght 515 nm. Right: Coomassie Blue staining.
C – 500 ng; I – 500 ng; II – 250 ng; III – 200 ng; IV – 150 ng; V – 100 ng; VI – 50 ng of rhodesain. All samples except the first, control sample, contain 20 µM (abundance) of compound **40**.

In this gel, we can see a band of the fluorescently labeled rhodesain weakening with the enzyme concentration at approximately 25 kDa. This size corresponds to the actual size of the active rhodesain, which is approximately 23 kDa (The UniProt Consortium 2020). The limit concentration for detection rhodesain is 100 ng. The ideal rhodesain concentration, which shows the strong fluorescent band of rhodesain but does not exceed the saturation of the enzyme by the probe, yet, is 500 ng.

The gel was additionally stained with Coomassie Brillant Blue and nothing could be seen, which indicates that the fluorescent method is more sensitive.

The feasibility of direct in-gel fluorescence detection was proven to be successful, after the treatment of rhodesain with **40**, together with the establishment of the minimal and the ideal enzyme concentration and detection of the rhodesain molecular weight. The following step was to confirm the binding mode of **40**. The

competition experiment with the active-site-directed inhibitor **E-64** was performed.

The first SDS-PAGE competition assay was performed parallelly and under the same conditions as the first SDS-PAGE assay with various enzyme concentrations, adapted from Frizler *et al.* (2013). As in the first SDS-PAGE experiment shown in this thesis (**Figure 26**), also here the main fluorescent band is caused by an unknown element and is present over the entire width of the gel. Besides that, nothing was detected (**Figure 28**).

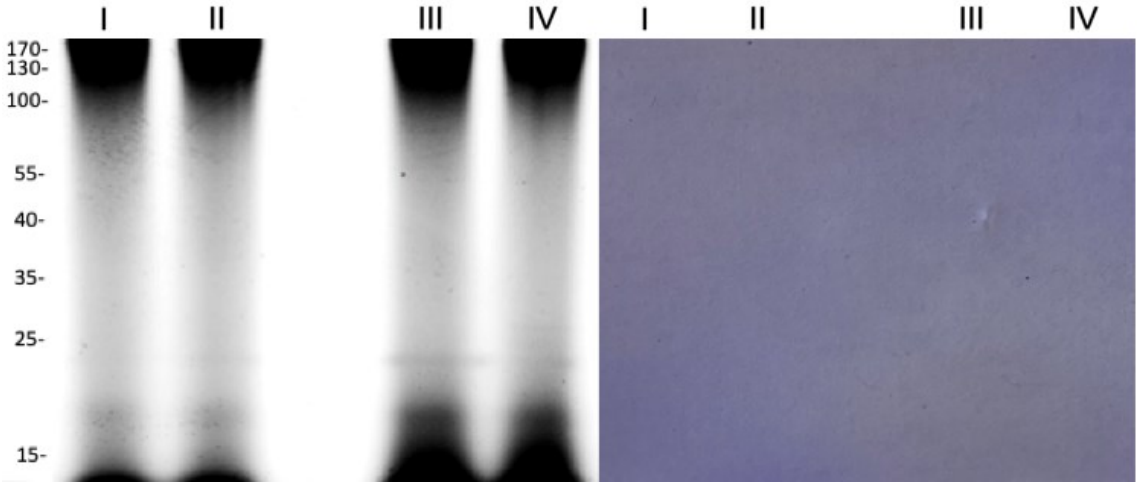

Figure 28. SDS-PAGE competition assay of **E-64** and **40** with DTT.
Left: ChemiDoc detection image, excitation wavelenght 485 nm, emission wavelenght 515 nm. Right: Coomassie Blue staining.
I – negative control; II – **E-64**; III – **E-64**, **40**; IV – **40.** All samples contain 500 ng of rhodesain. Concentration of each inhibitor in the sample is 20 µM.

The next experiment was performed with the same assay conditions as in the successful experiment without previous activation of rhodesain, adapted from Mertens *et al.* (2014) (**Figure 29**).

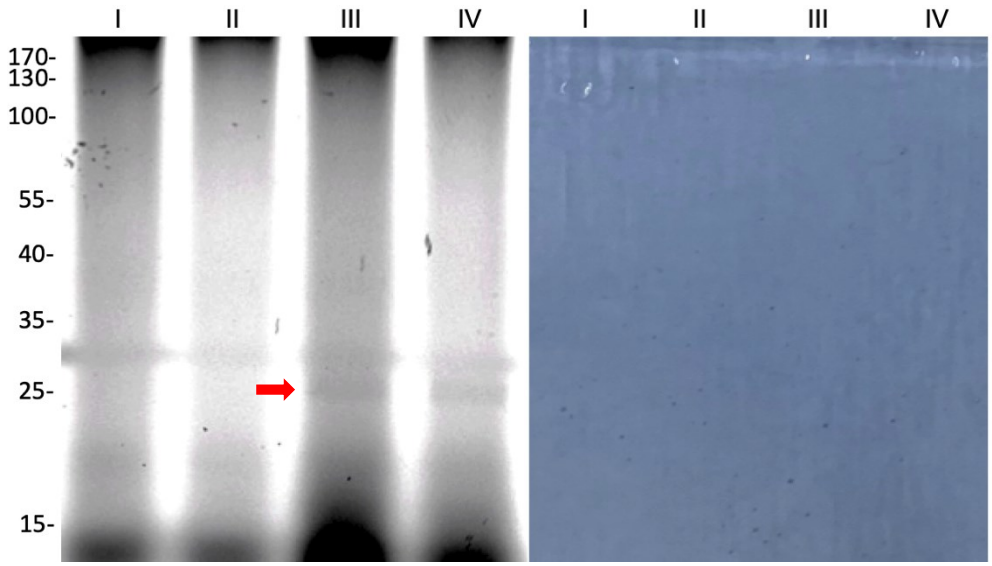

Figure 29. SDS-PAGE competition assay of **E-64** and **40.**

Left: ChemiDoc detection image, excitation wavelenght 485 nm, emission wavelenght 515 nm. Right: Coomassie Blue staining.

I – negative control; II – **E-64**; III – **E-64**, **40**; IV – **40**

All samples contain 500 ng of rhodesain. Concentration of each inhibitor in the sample is 20 µM.

A strong fluorescent band was observed in both samples containing rhodesain and activity-based probe **40**. The fact, that rhodesain is fluorescently labeled also in the sample, which was preincubated with active-site-directed, covalent-binding inhibitor, **E-64**, does not confirm the proposed hypothesis of covalent binding of compound **40** into the active-site of the enzyme. Nevertheless, it cannot be disapproved, because it is still possible, that **40** interacts with the surface nucleophiles of the protein and also with the active-site, if free.

The last experiment was performed to find out whether our compound is a selective inhibitor or a promiscuous binder. Compound **40** was applied to label rhodesain in the mixture with a complex proteome, lysate from human embryonic kidney 293 cells (HEK cell) provided by Martin Mangold. Rhodesain (200 ng) was incubated at 25 °C in 4 aliquots containing 2% DMSO, assay buffer (50 mM sodium acetate pH 5.5, 200 mM NaCl, 5 mM EDTA, 0,005% Brij 35) together with or without HEK cell lysate (4 µg) and **40** (20 µM) with the total volume of 40 µL. After 1 hour, 8 µL of the loading dye was added into the solutions and all of them

were denatured at 95 °C for 5 minutes. The samples were carefully pipetted into gel wells. Thereafter, a voltage of 120 V was applied until the loading dye reached approximately 1.5 cm from the end. The gel was then analyzed using ChemiDoc by Bio-Rad. The assay conditions were adapted from Frizler *et al.* (2013) and Mertens *et al.* (2014). The concentration of protein in HEK cell lysate was quantified by the Roti®-Nanoquant protein quantification assay.

In rhodesain, compound **40** has bound into its usual place, but in the sample where rhodesain is in the mixture with the proteins of HEK cell lysate, the compound has bound unspecifically to several other proteins rather than to rhodesain (**Figure 30**, lane **III**). The gel has been additionally stained with Coomassie Blue. Only proteins of HEK cell lysate, which were used in a significant abundance compared to the amount of rhodesain, are visible. This experiment unfortunately proves, that the compound **40** cannot be used as a reporter of rhodesain nor its inhibitor in human, because there are several other proteins, which would react with this probe.

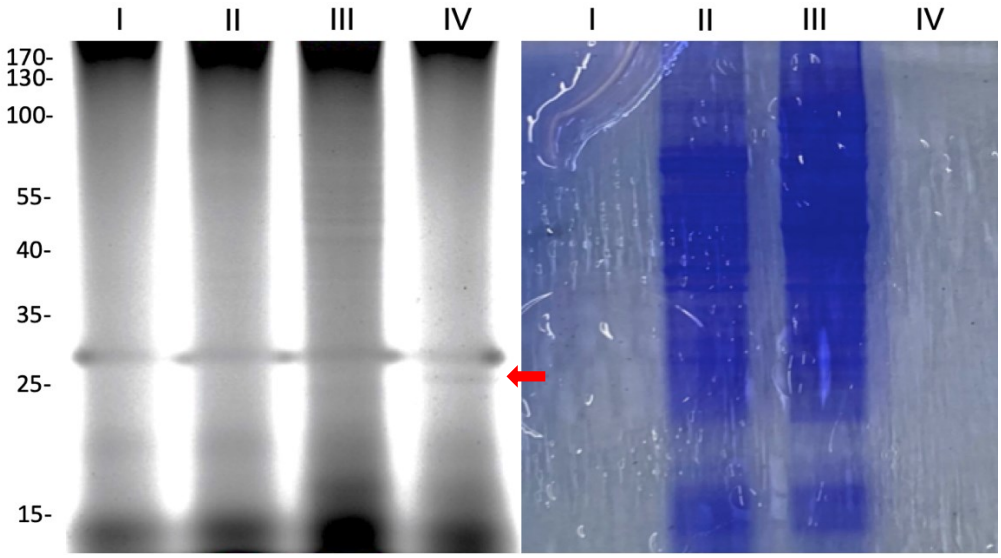

Figure 30. Imaging of rhodesain with the fluorescent probe **40** in the presence of HEK cell lysate.

Left: ChemiDoc detection image, excitation wavelenght 485 nm, emission wavelenght 515 nm. Right: Coomassie Blue staining.

I – negative control; II – HEK cell; III – HEK cell, **40**; IV – **40.**

All samples contain 200 ng of rhodesain. Concentration of the inhibitor is 20 µM. The amount of HEK cell lysate in a sample was 4 µg.

Further efforts should be made to prepare an activity-based probe for this protozoal cathepsin, as it may help to understand the disease mechanism better, through the visualization of the enzyme in native material. One of possible improvements could be a more specific inhibitor with, *e.g.*, different irreversible warhead. Another possibility is to change incubation conditions or read-out modality.

7. CONCLUSION

In summary, two weak, reversible inhibitors (**10** and **16**) of cathepsin S, which do not share any similarities in variable substituents, have been revealed among nifedipine derivatives.

Some inhibitors of cathepsin K have been discovered. The most potent one was the compound **19**, which is a peptidic Michael acceptor bearing a fluorophore. This compound consists of a substituted vinyl sulfonamide warhead, L-leucine in P2 position and a fluorescent dye, cyanine-5, hence, could be further investigated as an activity-based probe for cathepsin K.

The compound **21** has been identified as a reversible inhibitor of cathepsin L. For the kinetic evaluation, a stoichiometric paremeter, correcting the plot of steady-state velocities of the substrate hydrolysis against increasing concentrations of the inhibitor was used, resulting in the so-called three-parameter model.

The Michaelis-Menten value for spectrophotometric assays with rhodesain has been stated to 3.9 ± 0.6 µM under the herein reported assay conditions for the substrate Z-Phe-Arg-pNA.

The inhibitory potency of the reference inhibitor **E-64** against rhodesain has been determined. The second-order rate constant (k_{inact}/K_i) is 146 654 ± 82 760 $M^{-1}s^{-1}$.

The compound **36** inhibits rhodesain to almost the same extent as **E-64**, while being highly selective. This peptidic Michael acceptor bears an electrophilic vinyl sulfone warhead and phenylalanine in P2 position, with the terminal amine protected by *tert*-butyloxycarbonyl (Boc). Its derivatives, compounds **37** (methyl in *para* position) and **38** (chlorine in *meta* position) have a lower k_{inact}/K_i with a higher systematic error, but the remaining enzyme activities when using 10 µM of the inhibitor, were even a little lower. Nevertheless, all of them were around 0%.

Two activity-based probes for rhodesain were investigated. The compound **39** has exhibited slow-binding behavior and has been evaluated using appropriate parameters. Compound **40** was chosen to be used as an activity-based probe in sodium dodecyl sulfate polyacrylamide gel electrophoresis for labeling purposes of rhodesain. This compound has shown that it cannot be used in activity-based proteomics for rhodesain, because of being a promiscuous binder. However, the assay conditions have been improved and will be prepared for the next potential activity-based probe for rhodesain.

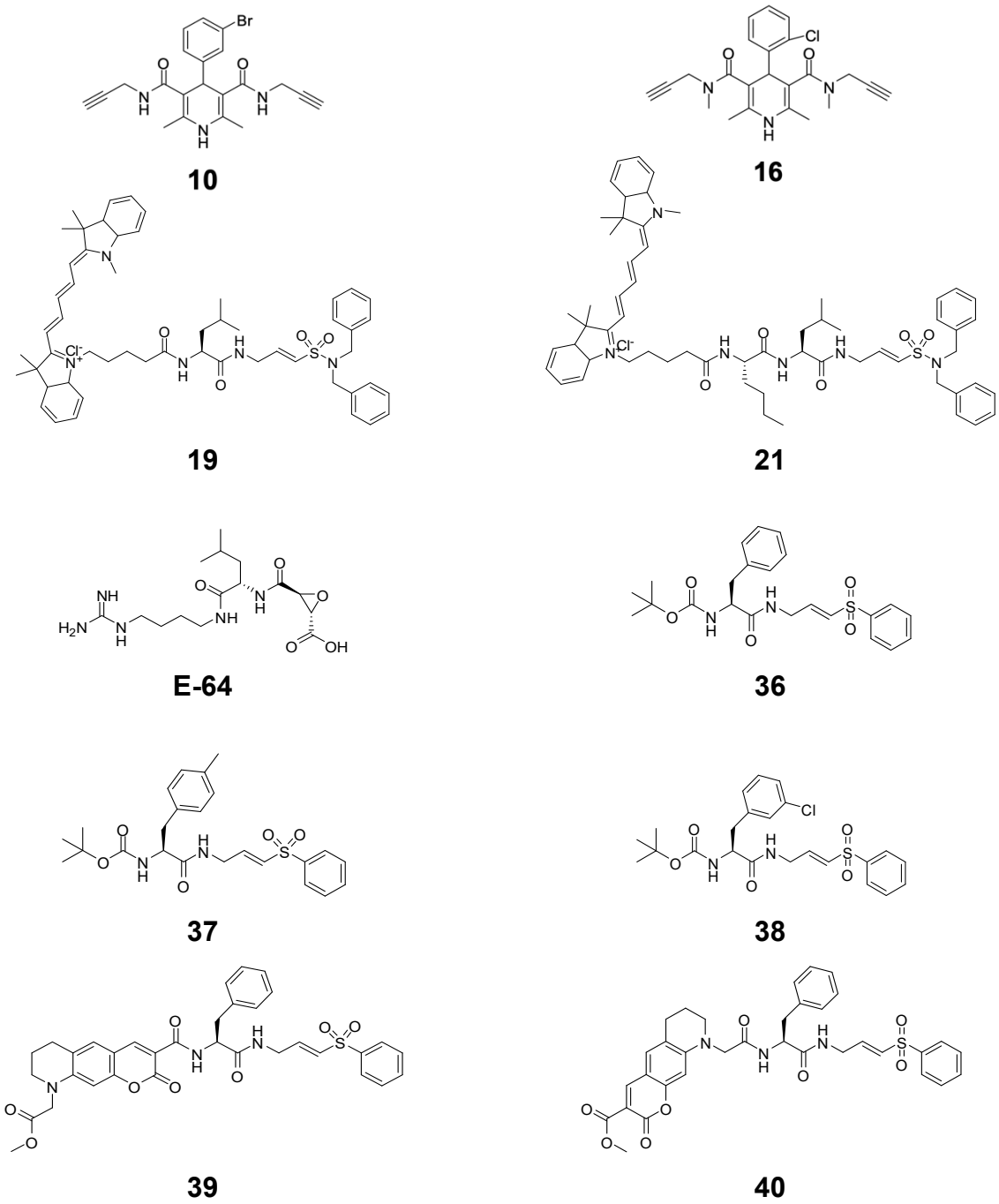

Figure 31. Discussed structures.

8. LIST OF FIGURES

9. LIST OF TABLES

10. LIST OF SCHEMES

11. REFERENCES

1. Ahn T, Yun CH. Molecular mechanisms regulating the mitochondrial targeting of microsomal cytochrome P450 enzymes. Curr Drug Metab. 2010;11(10):830-8.
2. Araujo TF, Cordeiro AV, Vasconcelos DAA, Vitzel KF, Silva VRR. The role of cathepsin B in autophagy during obesity: A systematic review. Life Sciences. 2018;209:274-81.
3. Barrett AJ, Rawlings ND, Salvesen G, Woessner JF. Handbook of Proteolytic Enzymes. 3rd ed. London, UK: Academic Press, Elsevier; 2013. li-liv p.
4. Barry ZT, Platt MO. Cathepsin S cannibalism of cathepsin K as a mechanism to reduce type I collagen degradation. J Biol Chem. 2012;287(33):27723-30.
5. Berg JM, Tymoczko JL, Gatto GJ, Stryer L. Biochemistry. 8th ed. New York: W.H. Freeman; 2015.
6. Berger A, Schechter I. Mapping the active site of papain with the aid of peptide substrates and inhibitors. Philos Trans R Soc Lond B Biol Sci. 1970;257(813):249-64.
7. Bhatt SM. Enzymology and Enzyme Technology: S. Chand; 2001.
8. Bromme D, Klaus JL, Okamoto K, Rasnick D, Palmer JT. Peptidyl vinyl sulphones: a new class of potent and selective cysteine protease inhibitors: S2P2 specificity of human cathepsin O2 in comparison with cathepsins S and L. Biochem J. 1996;315 (Pt 1):85-9.
9. Bromme D, Okamoto K, Wang BB, Biroc S. Human cathepsin O2, a matrix protein-degrading cysteine protease expressed in osteoclasts. Functional expression of human cathepsin O2 in Spodoptera frugiperda and characterization of the enzyme. J Biol Chem. 1996;271(4):2126-32.
10. Brun R, Blum J, Chappuis F, Burri C. Human African trypanosomiasis. Lancet. 2010;375(9709):148-59.
11. Caffrey CR, Hansell E, Lucas KD, Brinen LS, Alvarez Hernandez A, Cheng J, et al. Active site mapping, biochemical properties and subcellular localization

of rhodesain, the major cysteine protease of Trypanosoma brucei rhodesiense. Mol Biochem Parasitol. 2001;118(1):61-73.

12. Clark AK, Wodarski R, Guida F, Sasso O, Malcangio M. Cathepsin S release from primary cultured microglia is regulated by the P2X7 receptor. Glia. 2010;58(14):1710-26.

13. The UniProt Consortium. UniProt: a worldwide hub of protein knowledge 2020. Available from: https://www.uniprot.org/uniprot/Q95PM0.

14. Copeland RA. Evaluation of enzyme inhibitors in drug discovery. A guide for medicinal chemists and pharmacologists. Methods Biochem Anal. 2005;46:1-265.

15. Cravatt BF, Wright AT, Kozarich JW. Activity-based protein profiling: from enzyme chemistry to proteomic chemistry. Annu Rev Biochem. 2008;77:383-414.

16. Delaune KP, Alsayouri K. Physiology, Noncompetitive Inhibitor. StatPearls Publishing, Treasure Island (FL); 2019.

17. Doležal M *et al.* Farmaceutická chemie léčiv ovlivňujících centrální nervový systém: Karolinum; 2016.

18. Drake FH, Dodds RA, James IE, Connor JR, Debouck C, Richardson S, et al. Cathepsin K, but not cathepsins B, L, or S, is abundantly expressed in human osteoclasts. J Biol Chem. 1996;271(21):12511-6.

19. Drawz SM, Bethel CR, Doppalapudi VR, Sheri A, Pagadala SR, Hujer AM, et al. Penicillin sulfone inhibitors of class D beta-lactamases. Antimicrob Agents Chemother. 2010;54(4):1414-24.

20. Ebert MP, Kruger S, Fogeron ML, Lamer S, Chen J, Pross M, et al. Overexpression of cathepsin B in gastric cancer identified by proteome analysis. Proteomics. 2005;5(6):1693-704.

21. Ekkebus R, van Kasteren SI, Kulathu Y, Scholten A, Berlin I, Geurink PP, et al. On terminal alkynes that can react with active-site cysteine nucleophiles in proteases. J Am Chem Soc. 2013;135(8):2867-70.

22. Ettari R, Previti S, Tamborini L, Cullia G, Grasso S, Zappala M. The Inhibition of Cysteine Proteases Rhodesain and TbCatB: A Valuable Approach to Treat Human African Trypanosomiasis. Mini Rev Med Chem. 2016;16(17):1374-91.

23. Felix A, Moroder L, Toniolo C. Houben-Weyl Methods of Organic Chemistry. Stuttgart: Thieme; 2004.

24. Fernandez PL, Farre X, Nadal A, Fernandez E, Peiro N, Sloane BF, et al. Expression of cathepsins B and S in the progression of prostate carcinoma. Int J Cancer. 2001;95(1):51-5.
25. Frizler M. Development of Selective Nitrile Inhibitors and 'Activity-Based' Probes For Human Cathepsins K and S [Dissertation thesis]: Rheinische Friedrich-Wilhelms-Universität Bonn; 2012.
26. Frizler M, Lohr F, Furtmann N, Klas J, Gütschow M. Structural optimization of azadipeptide nitriles strongly increases association rates and allows the development of selective cathepsin inhibitors. J Med Chem. 2011;54(1):396-400.
27. Frizler M, Yampolsky IV, Baranov MS, Stirnberg M, Gutschow M. Chemical introduction of the green fluorescence: imaging of cysteine cathepsins by an irreversibly locked GFP fluorophore. Org Biomol Chem. 2013;11(35):5913-21.
28. Galmozzi A, Dominguez E, Cravatt BF, Saez E. Application of activity-based protein profiling to study enzyme function in adipocytes. Methods Enzymol. 2014;538:151-69.
29. Georgakis N, Ioannou E, Varotsou C, Premetis G, Chronopoulou EG, Labrou NE. Determination of Half-Maximal Inhibitory Concentration of an Enzyme Inhibitor. Methods Mol Biol. 2020;2089:41-6.
30. Giles NM, Watts AB, Giles GI, Fry FH, Littlechild JA, Jacob C. Metal and Redox Modulation of Cysteine Protein Function. Chem Biol. 2003;10(8):677-93.
31. Giroud M, Kuhn B, Saint-Auret S, Kuratli C, Martin RE, Schuler F, et al. 2H-1,2,3-Triazole-Based Dipeptidyl Nitriles: Potent, Selective, and Trypanocidal Rhodesain Inhibitors by Structure-Based Design. Journal of Medicinal Chemistry. 2018;61(8):3370-88.
32. Gocheva V, Zeng W, Ke D, Klimstra D, Reinheckel T, Peters C, et al. Distinct roles for cysteine cathepsin genes in multistage tumorigenesis. Genes Dev. 2006;20(5):543-56.
33. Gopinathan A, Denicola GM, Frese KK, Cook N, Karreth FA, Mayerle J, et al. Cathepsin B promotes the progression of pancreatic ductal adenocarcinoma in mice. Gut. 2012;61(6):877-84.
34. Gütschow M, Neumann U. Novel Thieno[2,3-d][1,3]oxazin-4-ones as Inhibitors of Human Leukocyte Elastase. Journal of Medicinal Chemistry. 1998;41(10):1729-40.

35. Hanada K, Tamai M, Yamagishi M, Ohmura S, Sawada J, Tanaka I. Isolation and Characterization of E–64, a New Thiol Protease Inhibitor. Agricultural and Biological Chemistry. 1978;42(3):523-8.
36. Herszenyi L, Plebani M, Carraro P, De Paoli M, Roveroni G, Cardin R, et al. The role of cysteine and serine proteases in colorectal carcinoma. Cancer. 1999;86(7):1135-42.
37. Hsing LC, Kirk EA, McMillen TS, Hsiao S-H, Caldwell M, Houston B, et al. Roles for cathepsins S, L, and B in insulitis and diabetes in the NOD mouse. J Autoimmun. 2010;34(2):96-104.
38. Huang X, Vaag A, Carlsson E, Hansson M, Ahren B, Groop L. Impaired cathepsin L gene expression in skeletal muscle is associated with type 2 diabetes. Diabetes. 2003;52(9):2411-8.
39. Hughes SJ, Glover TW, Zhu XX, Kuick R, Thoraval D, Orringer MB, et al. A novel amplicon at 8p22-23 results in overexpression of cathepsin B in esophageal adenocarcinoma. Proc Natl Acad Sci U S A. 1998;95(21):12410-5.
40. Chen B, Platt MO. Multiplex zymography captures stage-specific activity profiles of cathepsins K, L, and S in human breast, lung, and cervical cancer. J Transl Med. 2011;9:109.
41. Cheng Y, Prusoff WH. Relationship between the inhibition constant (K1) and the concentration of inhibitor which causes 50 per cent inhibition (I50) of an enzymatic reaction. Biochem Pharmacol. 1973;22(23):3099-108.
42. Illy C, Quraishi O, Wang J, Purisima E, Vernet T, Mort JS. Role of the occluding loop in cathepsin B activity. J Biol Chem. 1997;272(2):1197-202.
43. Inamdar S, T, A. Biochemical Engineering: Principles and Concepts. 3rd ed. New Delhi: PHI Learning Private Limited; 2012.
44. Jadhav PK, Schiffler MA, Gavardinas K, Kim EJ, Matthews DP, Staszak MA, et al. Discovery of Cathepsin S Inhibitor LY3000328 for the Treatment of Abdominal Aortic Aneurysm. ACS Med Chem Lett. 2014;5(10):1138-42.
45. Jaishankar P, Hansell E, Zhao DM, Doyle PS, McKerrow JH, Renslo AR. Potency and selectivity of P2/P3-modified inhibitors of cysteine proteases from trypanosomes. Bioorg Med Chem Lett. 2008;18(2):624-8.
46. Kamphuis IG, Kalk KH, Swarte MB, Drenth J. Structure of papain refined at 1.65 A resolution. J Mol Biol. 1984;179(2):233-56.

47. Kar NC, Pearson CM. Muscular dystrophy and activation of proteinases. Muscle Nerve. 1978;1(4):308-13.

48. Carl Roth GmbH + Co. KG. Roti®-Nanoquant, Protein quantitation assay, Instruction for use 2017. Available from: https://www.carlroth.com/medias/BA-K880-EN.pdf?context=bWFzdGVyfGluc3RydWN0aW9uc3wxMzg0OTN8YXBwbGljYXRpb24vcGRmfGluc3RydWN0aW9ucy9oZGEvaDFhLzg5MzM1NDYxNjQyNTQucGRmfGIxNzJjZjZmNjY4YTI4ODdjOTdmNmU4ODQ3ODc4MThjMWRiYjEzZmQ5MmJiYjMxYjg5ZTE4NDk2NGE0MjA5NzI.

49. Khan MY. The role of 'pro-sequences' in protein folding. Current Science. 1993;65(2):157-9.

50. Klein P, Johe P, Wagner A, Jung S, Kuhlborn J, Barthels F, et al. New Cysteine Protease Inhibitors: Electrophilic (Het)arenes and Unexpected Prodrug Identification for the Trypanosoma Protease Rhodesain. Molecules. 2020;25(6).

51. Kos J, Werle B, Lah T, Brunner N. Cysteine proteinases and their inhibitors in extracellular fluids: markers for diagnosis and prognosis in cancer. Int J Biol Markers. 2000;15(1):84-9.

52. Kramer JW. Clinical Enzymology. In: Kaneko JJ, editor. Clinical Biochemistry of Domestic Animals. 3rd ed: Academic Press; 1980. p. 175-99.

53. Kramer L, Turk D, Turk B. The Future of Cysteine Cathepsins in Disease Management. Trends Pharmacol Sci. 2017;38(10):873-98.

54. Krippendorff BF, Neuhaus R, Lienau P, Reichel A, Huisinga W. Mechanism-based inhibition: deriving K(I) and k(inact) directly from time-dependent IC(50) values. J Biomol Screen. 2009;14(8):913-23.

55. Lah TT, Kos J, Blejec A, Frkovic-Georgio S, Golouh R, Vrhovec II, et al. The Expression of Lysosomal Proteinases and Their Inhibitors in Breast Cancer: Possible Relationship to Prognosis of the Disease. Pathol Oncol Res. 1997;3(2):89-99.

56. Lecaille F, Kaleta J, Bromme D. Human and parasitic papain-like cysteine proteases: their role in physiology and pathology and recent developments in inhibitor design. Chem Rev. 2002;102(12):4459-88.

57. Ledvina M, Stoklasová A, Cerman J. Biochemie pro studující medicíny 1. díl. Prague: Karolinum; 2009.

58. Littlewood-Evans AJ, Bilbe G, Bowler WB, Farley D, Wlodarski B, Kokubo T, et al. The osteoclast-associated protease cathepsin K is expressed in human breast carcinoma. Cancer Res. 1997;57(23):5386-90.
59. Lonsdale-Eccles JD, Grab DJ. Trypanosome hydrolases and the blood-brain barrier. Trends Parasitol. 2002;18(1):17-9.
60. López-Otín C, Bond JS. Proteases: multifunctional enzymes in life and disease. J Biol Chem. 2008;283(45):30433-7.
61. Lorsch JR. Practical steady-state enzyme kinetics. Methods Enzymol. 2014;536:3-15.
62. Loser R, Pietzsch J. Cysteine cathepsins: their role in tumor progression and recent trends in the development of imaging probes. Front Chem. 2015;3:37.
63. Lv BJ, Lindholt JS, Wang J, Cheng X, Shi GP. Plasma levels of cathepsins L, K, and V and risks of abdominal aortic aneurysms: a randomized population-based study. Atherosclerosis. 2013;230(1):100-5.
64. Manchanda M, Das P, Gahlot GPS, Singh R, Roeb E, Roderfeld M, et al. Cathepsin L and B as Potential Markers for Liver Fibrosis: Insights From Patients and Experimental Models. Clin Transl Gastroenterol. 2017;8(6):e99.
65. Marasović M, Marasović T, Milos M. Robust Nonlinear Regression in Enzyme Kinetic Parameters Estimation. Journal of Chemistry. 2017;2017:1-12.
66. Matsumoto K, Mizoue K, Kitamura K, Tse WC, Huber CP, Ishida T. Structural basis of inhibition of cysteine proteases by E-64 and its derivatives. Biopolymers. 1999;51(1):99-107.
67. McPherson RA, Pincus MR. Henry's Clinical Diagnosis and Management by Laboratory Methods. 23rd ed. India: Elsevier; 2017.
68. Meisenberg G, Simmons W. Principles of Medical Biochemistry. Philadelphia: Saunders; 2011.
69. Mertens MD, Schmitz J, Horn M, Furtmann N, Bajorath J, Mares M, et al. A coumarin-labeled vinyl sulfone as tripeptidomimetic activity-based probe for cysteine cathepsins. Chembiochem. 2014;15(7):955-9.
70. Nishimura F, Naruishi H, Naruishi K, Yamada T, Sasaki J, Peters C, et al. Cathepsin-L, a key molecule in the pathogenesis of drug-induced and I-cell disease-mediated gingival overgrowth: a study with cathepsin-L-deficient mice. Am J Pathol. 2002;161(6):2047-52.

71. Nixon RA, Cataldo AM, Mathews PM. The endosomal-lysosomal system of neurons in Alzheimer's disease pathogenesis: a review. Neurochem Res. 2000;25(9-10):1161-72.
72. Otto HH, Schirmeister T. Cysteine Proteases and Their Inhibitors. Chem Rev. 1997;97(1):133-72.
73. Palmer JT, Rasnick D, Klaus JL, Bromme D. Vinyl sulfones as mechanism-based cysteine protease inhibitors. J Med Chem. 1995;38(17):3193-6.
74. Ramon Y, Behar S, Kishon Y, Engelberg IS. Gingival hyperplasia caused by nifedipine--a preliminary report. Int J Cardiol. 1984;5(2):195-206.
75. Rawlings ND, Barrett AJ, Thomas PD, Huang X, Bateman A, Finn RD. The MEROPS database of proteolytic enzymes, their substrates and inhibitors in 2017 and a comparison with peptidases in the PANTHER database. Nucleic Acids Research. 2017;46(D1):D624-D32.
76. Robker RL, Russell DL, Espey LL, Lydon JP, O'Malley BW, Richards JS. Progesterone-regulated genes in the ovulation process: ADAMTS-1 and cathepsin L proteases. Proceedings of the National Academy of Sciences. 2000;97(9):4689-94.
77. Roskoski R. Modulation of Enzyme Activity. In: Enna SJ, Bylund DB, editors. xPharm: The Comprehensive Pharmacology Reference: Elsevier; 2008. p. 1-11.
78. Rossi A, Deveraux Q, Turk B, Sali A. Comprehensive search for cysteine cathepsins in the human genome. Biol Chem. 2004;385(5):363-72.
79. Sadaghiani AM, Verhelst SH, Bogyo M. Tagging and detection strategies for activity-based proteomics. Curr Opin Chem Biol. 2007;11(1):20-8.
80. Saftig P, Hunziker E, Everts V, Jones S, Boyde A, Wehmeyer O, et al. Functions of cathepsin K in bone resorption. Lessons from cathepsin K deficient mice. Adv Exp Med Biol. 2000;477:293-303.
81. Sculley MJ, Morrison JF, Cleland WW. Slow-binding inhibition: the general case. Biochim Biophys Acta. 1996;1298(1):78-86.
82. Sena BF, Figueiredo JL, Aikawa E. Cathepsin S As an Inhibitor of Cardiovascular Inflammation and Calcification in Chronic Kidney Disease. Front Cardiovasc Med. 2017;4:88.

83. Senkane K, Vinogradova EV, Suciu RM, Crowley VM, Zaro BW, Bradshaw JM, et al. The Proteome-Wide Potential for Reversible Covalency at Cysteine. Angew Chem Int Ed Engl. 2019;58(33):11385-9.
84. Serim S, Haedke U, Verhelst SH. Activity-based probes for the study of proteases: recent advances and developments. ChemMedChem. 2012;7(7):1146-59.
85. Shree T, Olson OC, Elie BT, Kester JC, Garfall AL, Simpson K, et al. Macrophages and cathepsin proteases blunt chemotherapeutic response in breast cancer. Genes Dev. 2011;25(23):2465-79.
86. Schmitz J. Synthesis and Biological Evaluation of Nitrile-Based Peptidomimetic Inhibitors for Cysteine Cathepsins [Disertation Thesis]. 2016: Rheinische Friedrich-Wilhelms-Universität Bonn; 2016.
87. Schneider EV, Bottcher J, Huber R, Maskos K, Neumann L. Structure-kinetic relationship study of CDK8/CycC specific compounds. Proc Natl Acad Sci U S A. 2013;110(20):8081-6.
88. Siklos M, BenAissa M, Thatcher GR. Cysteine proteases as therapeutic targets: does selectivity matter? A systematic review of calpain and cathepsin inhibitors. Acta Pharm Sin B. 2015;5(6):506-19.
89. Silverman RB. Chapter 5 - Enzyme Inhibition and Inactivation. In: Silverman RB, editor. The Organic Chemistry of Drug Design and Drug Action (Second Edition). San Diego: Academic Press; 2004. p. 227-321.
90. Simpson RJ. Rapid coomassie blue staining of protein gels. Cold Spring Harb Protoc. 2010;2010(4):pdb prot5413.
91. Singh J, Petter RC, Baillie TA, Whitty A. The resurgence of covalent drugs. Nat Rev Drug Discov. 2011;10(4):307-17.
92. Sisay MT, Hautmann S, Mehner C, König GM, Bajorath J, Gütschow M. Inhibition of human leukocyte elastase by brunsvicamides a-C: cyanobacterial cyclic peptides. ChemMedChem. 2009;4(9):1425-9.
93. Skrzypczak M, Springwald A, Lattrich C, Haring J, Schuler S, Ortmann O, et al. Expression of cysteine protease cathepsin L is increased in endometrial cancer and correlates with expression of growth regulatory genes. Cancer Invest. 2012;30(5):398-403.
94. Smith HJ, Simons C. Proteinase and Peptidase Inhibition: Recent Potential Targets for Drug Development: Taylor & Francis 2002.

95. Srinivasan B, Forouhar F, Shukla A, Sampangi C, Kulkarni S, Abashidze M, et al. Allosteric regulation and substrate activation in cytosolic nucleotidase II from Legionella pneumophila. FEBS J. 2014;281(6):1613-28.
96. Steele RM, Schuna AA, Schreiber RT. Calcium antagonist-induced gingival hyperplasia. Ann Intern Med. 1994;120(8):663-4.
97. Steverding D, Sexton DW, Wang X, Gehrke SS, Wagner GK, Caffrey CR. Trypanosoma brucei: chemical evidence that cathepsin L is essential for survival and a relevant drug target. Int J Parasitol. 2012;42(5):481-8.
98. Stoeckle C, Quecke P, Ruckrich T, Burster T, Reich M, Weber E, et al. Cathepsin S dominates autoantigen processing in human thymic dendritic cells. J Autoimmun. 2012;38(4):332-43.
99. Taglieri N, Koenig W, Kaski JC. Cystatin C and cardiovascular risk. Clin Chem. 2009;55(11):1932-43.
100. Tonge PJ. Quantifying the Interactions between Biomolecules: Guidelines for Assay Design and Data Analysis. ACS Infect Dis. 2019;5(6):796-808.
101. Turk B, Bieth JG, Bjork I, Dolenc I, Turk D, Cimerman N, et al. Regulation of the activity of lysosomal cysteine proteinases by pH-induced inactivation and/or endogenous protein inhibitors, cystatins. Biol Chem Hoppe Seyler. 1995;376(4):225-30.
102. Turk V, Brzin J, Kotnik M, Lenarcic B, Popovic T, Ritonja A, et al. Human cysteine proteinases and their protein inhibitors stefins, cystatins and kininogens. Biomed Biochim Acta. 1986;45(11-12):1375-84.
103. Turk V, Stoka V, Vasiljeva O, Renko M, Sun T, Turk B, et al. Cysteine cathepsins: from structure, function and regulation to new frontiers. Biochim Biophys Acta. 2012;1824(1):68-88.
104. Varughese KI, Ahmed FR, Carey PR, Hasnain S, Huber CP, Storer AC. Crystal structure of a papain-E-64 complex. Biochemistry. 1989;28(3):1330-2.
105. Verma S, Dixit R, Pandey KC. Cysteine Proteases: Modes of Activation and Future Prospects as Pharmacological Targets. Front Pharmacol. 2016;7:107.
106. Vidak E, Javorsek U, Vizovisek M, Turk B. Cysteine Cathepsins and their Extracellular Roles: Shaping the Microenvironment. Cells. 2019;8(3).

107. Vizovisek M, Fonovic M, Turk B. Cysteine cathepsins in extracellular matrix remodeling: Extracellular matrix degradation and beyond. Matrix Biol. 2019;75-76:141-59.
108. Waggoner A. Fluorescent labels for proteomics and genomics. Curr Opin Chem Biol. 2006;10(1):62-6.
109. Weber K, Osborn M. The reliability of molecular weight determinations by dodecyl sulfate-polyacrylamide gel electrophoresis. J Biol Chem. 1969;244(16):4406-12.
110. Wilkinson RD, Williams R, Scott CJ, Burden RE. Cathepsin S: therapeutic, diagnostic, and prognostic potential. Biol Chem. 2015;396(8):867-82.
111. Wu G, Yuan Y, Hodge CN. Determining appropriate substrate conversion for enzymatic assays in high-throughput screening. J Biomol Screen. 2003;8(6):694-700.
112. Wu T, Trevisan M, Genco RJ, Dorn JP, Falkner KL, Sempos CT. Periodontal disease and risk of cerebrovascular disease: the first national health and nutrition examination survey and its follow-up study. Arch Intern Med. 2000;160(18):2749-55.